



Copper(II) ion removal by chemically and physically modified sawdust biochar

Ahmed Eleryan¹ · Uyiosa O. Aigbe² · Kingsley E. Ukhurebor³ · Robert B. Onyancha⁴ · Tarek M. Eldeeb¹ · Mohamed A. El-Nemr⁵ · Mohamed A. Hassaan¹ · Safaa Ragab¹ · Otolorin A. Osibote² · Heri S. Kusuma⁶ · Handoko Darmokoesoemo⁷ · Ahmed El Nemr¹

Received: 14 April 2022 / Revised: 27 May 2022 / Accepted: 6 June 2022 / Published online: 21 June 2022
© The Author(s) 2022

Abstract

The difference between physical activations (by sonications) and chemical activations (by ammonia) on sawdust biochar has been investigated in this study by comparing the removal of Cu(II) ions from an aqueous medium by adsorption on sawdust biochar (SD), sonicated sawdust biochar (SSD), and ammonia-modified sawdust biochar (SDA) with stirring at room temperature, pH value of 5.5–6.0, and 200 rpm. The biochar was prepared by the dehydrations of wood sawdust by reflux with sulfuric acid, and the biochar formed has been activated physically by sonications and chemically by ammonia solutions and then characterized by the Fourier transform infrared (FTIR); Brunauer, Emmett, and Teller (BET); scanning electron microscope (SEM); thermal gravimetric analysis (TGA); and energy-dispersive spectroscopy (EDX) analyses. The removal of Cu(II) ions involves 100 mL of sample volume and initial Cu(II) ion concentrations (conc) 50, 75, 100, 125, 150, 175, and 200 mg L⁻¹ and the biochar doses of 100, 150, 200, 250, and 300 mg. The maximum removal percentage of Cu(II) ions was 95.56, 96.67, and 98.33% for SD, SSD, and SDA biochars, respectively, for 50 mg L⁻¹ Cu(II) ion initial conc and 1.0 g L⁻¹ adsorbent dose. The correlation coefficient (R^2) was used to confirm the data obtained from the isotherm models. The Langmuir isotherm model was best fitted to the experimental data of SD, SSD, and SDA. The maximum adsorption capacities (Q_m) of SD, SSD, and SDA are 91.74, 112.36, and 133.33 mg g⁻¹, respectively. The degree of fitting using the non-linear isotherm models was in the sequence of Langmuir (LNR) (ideal fit) > Freundlich (FRH) > Temkin (SD and SSD) and FRH (ideal fit) > LNR > Temkin (SDA). LNR and FRH ideally described the biosorption of Cu(II) ions to SD and SSD and SDA owing to the low values of χ^2 and R^2 obtained using the non-linear isotherm models. The adsorption rate was well-ordered by the pseudo-second-order (PSO) rate models. Finally, chemically modified biochar with ammonia solutions (SDA) enhances the Cu(II) ions' adsorption efficiency more than physical activations by sonications (SSD). Response surface methodology (RSM) optimization analysis was studied for the removal of Cu(II) ions using SD, SSD, and SDA biochars.

Keywords Environment · Biochar · Adsorption · Sawdust · Wastewater · Copper removal

Highlights

- The adsorption of Cu(II) ions by SD, SSD, and SDA was best modelled by Langmuir and PSO.
- SD, SSD, and SDA are effective and cheap biosorbents for the confiscations of Cu(II) ions.
- The impact on the sorptions efficiency of SD, SSD, and SDA was influenced by the pH.
- The Q_m for Cu(II) onto SD, SSD, and SDA was 91.74, 112.36, and 133.33 mg g⁻¹, respectively.

✉ Ahmed El Nemr
ahmedmoustafaelnemr@yahoo.com;
ahmed.m.elnemr@gmail.com

Extended author information available on the last page of the article

1 Introduction

Recently, increase in environmental contaminations was caused by the release of heavy metals (HMs) [1–3] such as arsenic (As), chromium (Cr), cadmium (Cd), copper (Cu), iron (Fe), lead (Pb), mercury (Hg), nickel (Ni), and zinc (Zn), grouped as inert chemicals [4–9] which are present in wastewater, and has an effect to humans and the environment [10, 11], dyes [12, 13], and other noxious materials, owing primarily to the incessant expansions of industrial activities and the massively increasing

human populations, as well as the continuous evolutions of technological advancements [14–18].

Globally, these increasing environmental contaminations or effluences are critical prompting several noxious wastes and agricultural and climatic difficulties that are antagonizing and detrimental to humans (health complications and otherwise), other living organisms, natural resources, and the entire aquatic, atmospheric, and terrestrial ecosystems [19, 20]. Organic and inorganic emissions from industrial activities, waste furnaces from industrial activities, use of fossil fuels from industrial activities and automobile exhausts, as well as the use of modern agricultural machinery appear to be some of the primary sources of these environmental contaminations or toxic wastes [21]. It is therefore evident that industries, especially those manufacturing industries such as mining, plating, electroplating, smelting, metallurgy, fertilizer, paper, refining, tanneries, wood, surface finishing, agrochemicals, and petrochemicals, use HMs during production and, in one form or the other, convey several noxious substances and other environmental effluences to the ecosystems (particularly the aquatic environment) during the process [22–26]. Supposedly, the industrial and agricultural sectors are to contribute suggestively to the rehabilitation and remediation progressions as well as be the frontier in the development, advancement, and management of the economy as well as society in general for environmental and agricultural sustainability.

Cu is believed to be one of the most widely utilized metals in several domains as well as in our daily activities as an ornament amongst all other HMs [27]. Cu is also being used in plating and electroplating, the manufacturing of brass, mining and smelting, petrochemical refining, as well as the manufacturing of in Cu-based agrochemicals, etc. The wastes from Cu(II) ions in the form of effluents or wastes from these manufacturing industries are released into the ecological environments in various quantities. These wastes end up endangering humans, other living organisms (animals and plants), and the entire ecosystem [28, 29]. Essentially, the extent of environmental contaminations from Cu(II) ions and other HMs in wastewater is determined primarily by the period and extent of the contaminations, as well as the actions that initiate the source of the contaminations [28, 30]. Elevated levels of Cu in the human blood could harm various key organs, including the liver, kidney, and pancreas, and cause reactive oxygen types, DNA, lipid, and protein impairments [22]. While in the aquatic ecosystem, they damage aquatic animals' critical organs (such as the liver, gills and kidneys) and systems (such as the neurological system), in addition to their sexual lives.

However, the permissible international extent of Cu(II) ions in drinking or domestic water according to international regulatory bodies (such as the USEPA, BIS, and WHO) varies between 1.30, 1.50, and 2.00 mg L⁻¹, respectively [28, 30].

Therefore, it is imperative to remove noxious HMs and other noxious materials from wastewater and the environment at large, to manage and mitigate the ensuing antagonizing and detrimental consequences. Accordingly, there are variously described, established, and reported technologies such as adsorption, biosorption, chemical precipitation, electrolytic recovery, flotations, and membrane separations for the control, rehabilitations, management, remediations, recovery, and sequestrations of HMs from the environment [31–38]. The adsorption process has been widely considered and described as one of the modern and most ecologically friendly techniques for removing and managing noxious HMs and other noxious materials from wastewaters ensuing from several industrial activities [28].

Several scientists have and are currently investigating low-cost (cheap) adsorbents with remarkable metal-binding abilities for wastewater management and treatment [2, 28, 29]. Correspondingly, it has been reported that a variety of agro-based by-products, such as fruit peelings, compost, seeds, and plant leaves, are nowadays widely used for wastewater treatment in the presence of HMs [2, 28, 29, 39]. The core components of flora cells are cellulose, lignin, and tannin, which have a high capacity for absorbing HM ions [5, 40]. Nonetheless, the focus of this research will be on the Cu adsorption and confiscation potentials in solutions (water), which, like all other HMs, are primarily derived from industrial activity. Nevertheless, few investigations on the adsorption capabilities of absorbing Cu(II) ions from aqueous solutions have been published [41–48]. The use of biosorption modified biochar, as well as the applications of physical and chemical activations, have progressively been implemented for the sustainable removal of noxious contaminated materials from aqueous solutions [49, 50].

As a result, the current study endeavoured to re-evaluate and re-explore the possibilities of using waste agro-based by-products as a natural adsorbent for Cu(II) ion removal. The basis for this study was to demonstrate the use of more readily available waste agro-based by-products as a natural for Cu(II) ion removal. The study will consider and focus on the difference between physical activations (by sonications) and chemical activation (by ammonia) on sawdust (SD) biochar by investigating the removal of Cu(II) ions from aqueous mediums comparatively by adsorption on SD, sonicated sawdust (SSD), and

ammonia-modified sawdust (SDA) biochar with stirring at room temperature, pH value of 5.5–6.0, and 200 rpm. The SD biochar was prepared by the dehydrations of wood saw via reflux with sulfuric acid, and the biochar formed was activated physically by sonications (SSD) and chemically by ammonia solutions (SDA). Besides, the experimental, characterization, and morphological studies using the FTIR, BET, SEM, TGA, XRD, and EDX analyser were systematically considered and emphasized.

2 Materials and methods

2.1 Materials and apparatus

Wood saw dust was obtained from a local wood market in Alexandria, Egypt, and was utilized as a raw material for preparing the biochar. Ammonia solution (NH_4OH , MWt = 35 g, assay 25%) was acquired from Sigma-Aldrich, USA. The standard stock solutions of Cu(II) (CuSO_4 , MWt = 249.69 g, assay 99%) was gotten from copper sulfate of Sigma-Aldrich, USA. Sodium diethyldithiocarbamate used as a chromogenic reagent for Cu(II) ion detections was acquired from BDH Chemicals LTD, Poole, UK. Pg instrument model T80 UV/Visible high-performance double-beam spectrophotometer matched with glass cells of 1 cm optical path, Shaker (A JS shaker (JSOS-500)), and pH meter JENCO (6173) were used in this study.

2.2 Methods

2.2.1 SD biochar preparations

The collected saw dust was thoroughly washed with tap water several times to remove dust and subsequently dried in an oven at 105 °C for 48 h. Two hundred and fifty grams of saw dust placed in 1000 mL solutions of 75% H_2SO_4 was boiled in a refluxed setting at 200 °C for 2 h, and then, the samples were sieved and washed with purified water until the washing solutions become neutral; thereafter, it was washed with ethanol. The final sample of biochar was then dried in an oven at a temperature of 105 °C; subsequently, its weight was measured (112 g). The acquired biochar from this process was labelled as SD.

2.2.2 SSD biochar preparations

The prepared SD biochar was suspended in water and subsequently subjected to ultrasonic energy for 30 min for physical activations. The sonicated solution was filtered

and washed with distilled water and dried at 105 °C. The obtained sonicated SD from this treatment was labelled as SSD [29].

2.2.3 Ammonia-modified SD biochar (SDA) preparations

The prepared SD was subsequently subjected to ammonium hydroxide (NH_4OH). For functionalized SD with NH_4OH , 20 g of prepared SD was boiled in a refluxed setting in a 100-mL solution of 25% NH_4OH for 120 min. After, it was cold filtered and washed with purified water and finally washed with ethanol. Lastly, the functionalized biochar was then dried at 105 °C for 48 h and was labelled as SDA [29].

2.3 Characterizations of biochars

The adsorption–desorption (A–D) isotherm of N_2 gas on biochar was attained at the boiling point of N_2 gas. The measurements of the BET surface area (S_{BET}) of the biochars were through the adsorption of nitrogen at 77 °K employing the surface area and pore analyser [51, 52], (BELSORP-Mini II, BEL Japan, Inc.). The investigations of the isotherm were undertaken by utilizing the BET plot in obtaining a monolayer volume (V_m) (cm^3 (STP) g^{-1}), the surface area (S_{BET}) ($\text{m}^2 \text{g}^{-1}$), total pore volume ($\text{cm}^3 \text{g}^{-1}$), energy constant (C), as well as the mean pore diameter (nm). Also, the micropore surface area (S_{mi}) and micropore volume (V_{mi}) along with the mesopore surface area (S_{mes}) and mesopore volume (V_{mes}) of biochars were obtained through the Barrett–Joyner–Halenda (BJH) technique [29, 53], in accordance with the BELSORP analysis software program. The pore size distributions were estimated from the desorption isotherm via the utilizations of the BJH technique. The surface morphology of biochars was considered through the SEM (QUANTA 250) together with the EDX that was carried out for the elemental investigations. The studies of the functional groups (FGs) on the biochar surface were carried out using the FTIR spectroscopy (VERTEX70 model) coupled with the Platinum ATR unit (model V-100) in detecting the IR-observable FGs on the biochar surface, with the wavelength number range ($400\text{--}4000 \text{ cm}^{-1}$). X-ray diffractograms (XRD) used a Bruker Meas Srv (D2 PHASER) (D2-208219)/D2-2082019 diffractometer operating at 30 kV and 10 mA with a Cu tube ($\lambda = 1.54$) and with a 2θ range of 5–80. The thermal analyses were executed by the SDT650-Simultaneous Thermal Analyser instrument in the range between 50 and 1000 °C utilizing a temperature of 5 °C for every 60 s as ramping temperature [29, 53].

Table 1 Range and levels used for the batch SD, SSD, and SDA adsorption studies

Biochar	Independent variable notations	Units	Minimum	Maximum	Mean	StD
SD	A: X1	g L^{-1}	1	3	2.08	0.85
	B: X2	mg L^{-1}	50	175	107.50	53.86
	C: X3	min	15	180	96.75	71.11
SSD	A: X1	g L^{-1}	1	3	1.95	0.89
	B: X2	mg L^{-1}	50	200	128.75	61.92
	C: X3	min	5	180	77.50	71.18
SDA	A: X1	g L^{-1}	1	3	2.05	0.84
	B: X2	mg L^{-1}	50	200	122.50	63.30
	C: X3	min	5	180	83.00	73.90

A, adsorbent dose; B, Cu^{2+} ion initial conc; C, contact time

2.4 Measurement adsorption for the divalent Cu

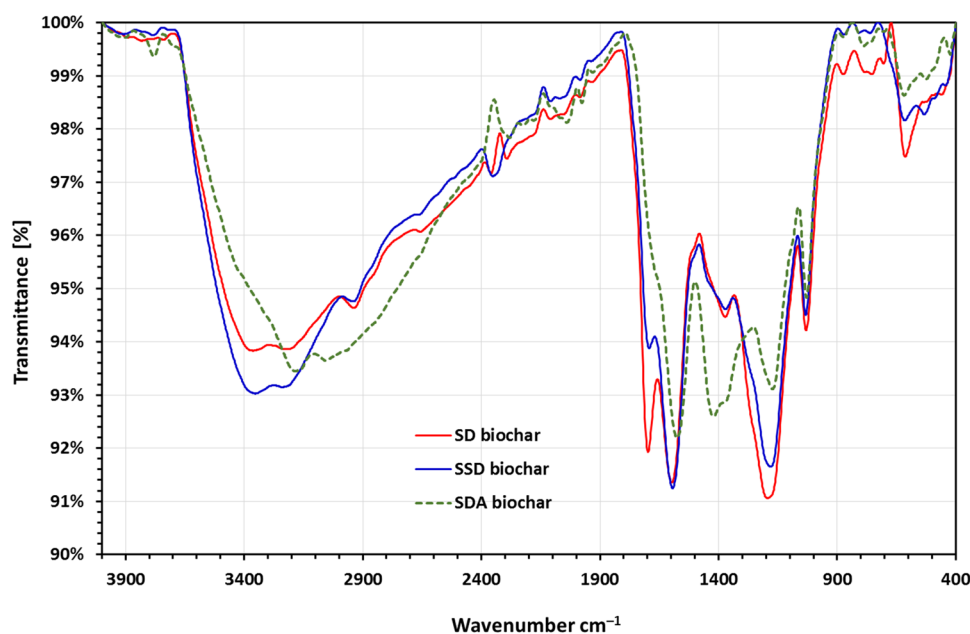
A stock solution of Cu(II) ions (1000 mg L^{-1}) was acquired by dissolving 3.921 g of $\text{CuSO}_4 \cdot 5\text{H}_2\text{O}$ in 1000 mL of purified water, and this solution was diluted to have the needed concentrations (conc) for the removal test as well as the standard curve. Batch adsorption experiments were undertaken to estimate the adsorption capability and thermodynamic and kinetic variables of the SD, SSD, and SDA which were acquired from sawdust [29]. A series of Erlenmeyer flasks (EFs) (300 mL) encompassing of 100 mL of various conc of Cu(II) ion solutions and varied quantities of biochar were stunned at 200 rpm for a specific durations. The sample pH was modified to the anticipated values with 0.1 M HCl or 0.1 M NaOH . Approximately 0.1 mL of the solutions in

the EFs was then detached from the adsorbent, and the conc of Cu(II) ions were determined at various intervals of time and equilibrium. The conc of Cu(II) ions were estimated via the spectrophotometry employing sodium diethyldithiocarbamate as a chromogenic agent ($\lambda_{\text{max}} = 460 \text{ nm}$) [29, 54].

Initially, the slope of the standard curve correlated between known Cu(II) ion conc and related absorbance was used to calculate the unknown Cu(II) ion conc (C_t) at time intervals from absorbance value practically detected. C_t calculations are carried out using Eq. (1).

$$C_t = \frac{\text{absorbance at interval time } t}{\text{slope of standard curve}} \quad (1)$$

Cu(II) ion conc at equilibrium C_e ; at stable values of absorbance, Eq. (2) shows C_e calculations.

Fig. 1 FTIR analysis of SD biochar, SSD biochar, SDA biochar

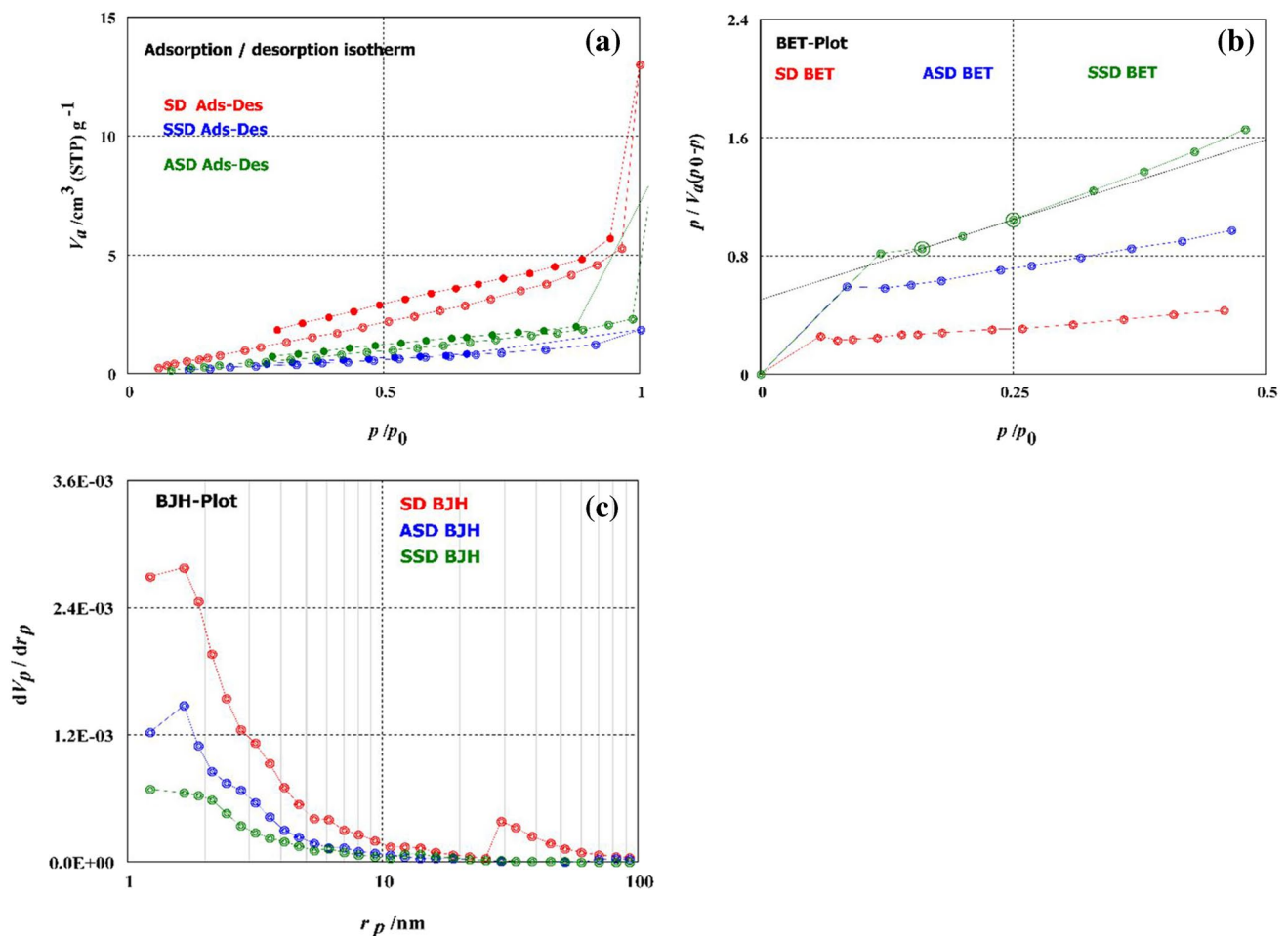


Fig. 2 **a** Adsorption–Desorption isotherm, **b** BET, and **c** BJH analyses of SD, SSD, and SDA biochars

$$C_e = \frac{\text{absorbance at equilibrium}}{\text{slope of standard curve}} \quad (2)$$

The adsorption capacities at equilibrium (q_e) were estimated using Eq. (3):

$$q_e = \frac{C_0 - C_e}{W} \times V \quad (3)$$

where q_e is the amount of metal per unit of adsorbent at equilibrium (mg g^{-1}); C_0 and C_e are the initial and equilibrium conc in the liquid phase (mg L^{-1}), respectively; and V is the volume of the solutions (L) while W is the mass of adsorbent (g) [29].

2.4.1 The impact of solutions pH

The impact of pH was undertaken by contacting 100 mL of 100 mg L^{-1} of initial Cu(II) ion conc at varying pH

of 1.50–5.5, with a fixed dosage of SD, SSD, and SDA biochars. Since Cu(II) ions precipitated at $\text{pH} > 6$, so the removal study was carried out at $\text{pH} 1.50$ – 5.5 [29].

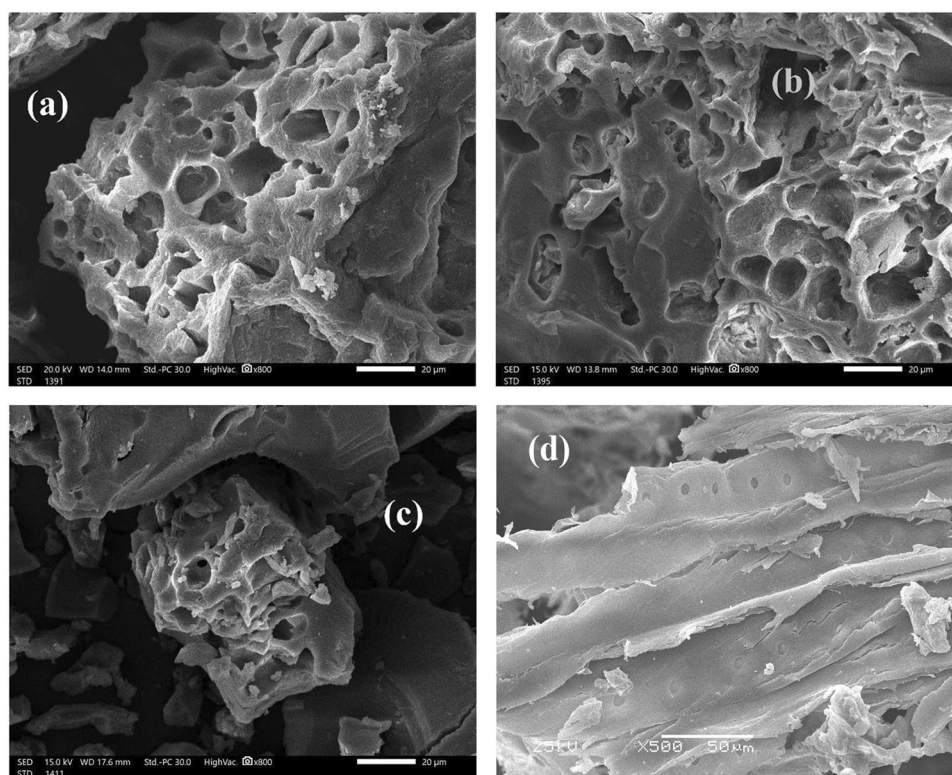
2.4.2 The impact of initial Cu(II) ion conc and adsorbent dosage

The isotherm study for saw dust biochars was carried out utilizing the various initial conc of Cu(II) ion solutions (50, 75, 100, 125, 150, 175, and 200 mg L^{-1}) which were contacted

Table 2 BJH data analysis of (a) SD, (b) SSD, and (c) SDA biochars

Biochar	$a_p; \text{m}^2 \text{ g}^{-1}$	$V_p; \text{m}^3 \text{ g}^{-1}$	r_p ; peak (area); nm
SD	3.5890	0.012872	1.22
SSD	4.5740	0.015620	1.22
SDA	3.2593	0.007689	1.66

Fig. 3 Scanning electron microscope analysis of **a** SDB, **b** SSDB, **c** SDAB, and **d** SD raw material



with different doses (1.0, 1.5, 2.0, 2.5, and 3.0 g L⁻¹) for SD biochar and (1.0, 1.5, 2.0, 2.5, and 3.0 g L⁻¹) for SSD and SDA biochars. The samples were shaken at 200 rpm, and the Cu(II) ion conc was analysed at different time intervals at room temperature (25 ± 2 °C) [29].

2.4.3 The impact of contact time

In the kinetics study, a changing dose of SD, SSD, and SDA biochars (1.0, 1.5, 2.0, 2.5, and 3.0 g L⁻¹) was added to EFs comprising 100 mL of sample volume; 50, 75, 100, 125, 175, and 200 mg L⁻¹ of initial Cu(II) concentrations were shaken at 200 rpm. Samples were withdrawn from the solutions at various intervals of time, and the residual conc of Cu(II) ions left in the solutions were then analyzed [29].

2.5 Optimization study RSM

Optimal designs are very adaptable and can handle various operator limitations and other complicated experimental design issues like constrained designed regions, various levels, and limits on the overall amount of experimental runs. These designs are mathematically created designs which seek to reduce a particular optimality measure to opt for a near-optimal design. The mathematical measure focuses on the regression coefficient estimation or the response variable in the design region prediction employing the optimality conditions [55].

The D-optimal design was employed to study the adsorption of Cu²⁺ ions from adsorbent coating using the State-Ease Design Expert v 13.0.5.0 software. Optimizations of effective parameters on the adsorption process,

Table 3 EDX analysis data of SD, SSD, and SDA biochars

Biochar	SD biochar		SSD biochar		SDA biochar	
	wt%	at.%	wt%	at.%	wt%	at.%
C	48.23	66.33	55.35	63.39	57.19	64.32
N	ND	ND	ND	ND	7.63	7.32
O	28.15	28.98	28.48	28.31	32.65	27.42
S	23.62	12.13	16.17	8.30	2.23	0.94

ND not detected

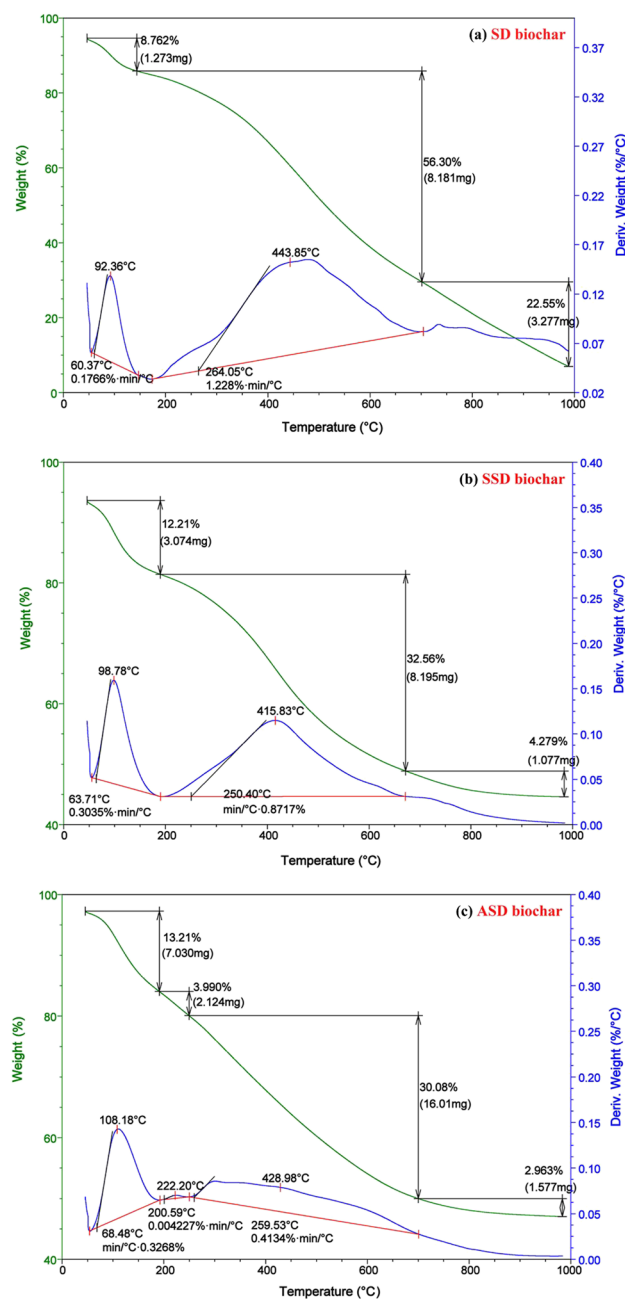


Fig. 4 Thermal gravimetrical analysis of **a** SD biochar, **b** SSD biochar, and **c** SDA biochar

i.e. the impacts of the three independent variables (A: adsorbent dose, B: initial Cu^{2+} ion conc: and C: contact time) on the response (R: Cu^{2+} ions % of removal) were studied using the response surface methodology (RSM). The range and variable of the experiment are given in Table 1.

The optimal custom design for the A, B, and C was based on 6 axial points, 8 factorial points, and 6 replicates at the

central point. The number of experiments that were carried out was estimated by Eq. (4):

$$N = 2^k + 2k + C = 2^3 + 2 \cdot 3 + 6 = 20 \quad (4)$$

where N is the number of experiments that were carried out, K is the number of factors to be tested, and C is the number of experiments conducted at the centre. The lower and higher limits of each factor are shown in Table 1. The experiment data matrix was obtained using the State-Ease Design Expert v 13.0.5.0. The obtained model was statistically analysed by the analysis of variance (ANOVA). The interactions amongst the various variables were considered by employing the surface contour plots.

3 Results and discussions

3.1 The characterization of the biochars

3.1.1 Estimating biochar surface FGs by FTIR

FTIR analysis was performed on sawdust biochar and its modified derivatives for identifications of the FGs on their surfaces. Figure 1 shows FTIR spectra of SD, SSD, and SDA biochars. Bands at 3363 and 3353 cm^{-1} represent the O–H stretching vibrations and were noticed in SD and SSD biochars, respectively. While in SDA, a new weak band appeared at 3780 cm^{-1} representing (–NH) of the amino group, signifying that the NH_4OH modifications intensified the N–H FGs. The band at 3185 cm^{-1} represents the stretching of water dissociations and non-dissociations, while the band at 3056 cm^{-1} represents aromatic (=C–H) stretch. Bands appearing at 2941 and 2937 cm^{-1} in SD and SSD represent –C–H stretch of the alkyl. Weak bands from 2000 – 1665 cm^{-1} known as overtones were bands at 1967 cm^{-1} in SDA, 1697 cm^{-1} in SD, and 1692 cm^{-1} in SSD biochars. Respective bands at 1597 , 1593 and 1575 cm^{-1} in SD, SSD, and SDA biochars represent –C–C– stretch (in-ring) [56], while bands from 1500 to 1700 cm^{-1} represent amine N–H and carbonyl group $\text{C}=\text{O}$ [57]. The new band at 1422 cm^{-1} in SDA biochar represents C–O FGs. Bands at 1372 and 1371 cm^{-1} in SD and SSD biochars, which were noticed not to be present or extinct in SDA biochar, were allocated to the stretching vibrations of $-\text{N}=\text{C}=\text{O}$ FGs or primarily assigned to C–N stretching. The bands at 1193 , 1179 , and 1172 cm^{-1} in SD, SSD, and SDA biochars indicate the presence of oxygenated carbon chains C–O–C. The bands at 1030 , 1032 , and 1029 cm^{-1} in SD, SSD, and SDA were related to the C–O–H FGs [58–60].

Fig. 5 XRD analysis of SD biochar, SSD biochar, and SDA biochar

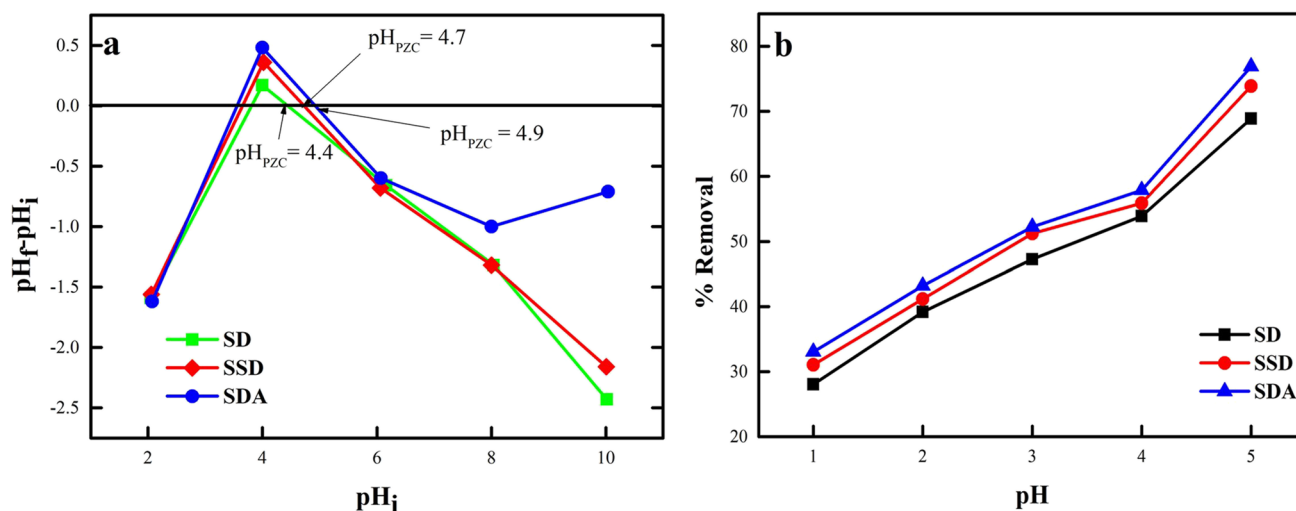
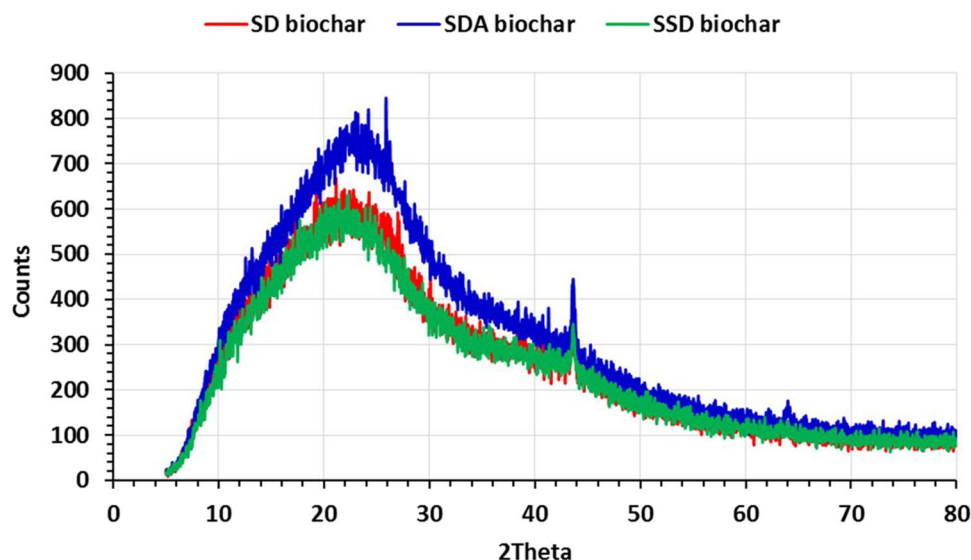


Fig. 6 **a** The pH_{PZC} of SD, SSD, and SDA biochars, and **b** impact of solutions pH on the Cu(II) ion removal using SD, SSD, and SDA biochars

3.1.2 The biochar surface analysis

The influence of sonications and ammonia solution treatment on the surface properties of wood SD was investigated by N_2 A–D, BET and BJH techniques were employed in estimating the specific characteristic of biochar surfaces. Figure 2 indicates that the BET specific surface area of biochars decreased as $SSD (4.0098 \text{ m}^2 \text{ g}^{-1}) > SDA (3.1926 \text{ m}^2 \text{ g}^{-1}) > SD (2.9136 \text{ m}^2 \text{ g}^{-1})$. It is noted that modifications increase the specific surface area, and the effect of physical modifications by sonications was more effective than chemical modifications

using ammonia. The mean pore diameter decreased with modifications in order $SD (16.824 \text{ nm}) > SSD (14.728 \text{ nm}) > SDA (8.3738 \text{ nm})$, and the effect of ammonia modifications is more than sonications on pore diameter decreasing due to $-NH_2$ and $-OH$ groups. The pore types are mesoporous (ranging between 20 and 50 nm). The total pore volume of SD, SSD, and SDA biochars were 12.24×10^{-3} , 14.76×10^{-3} , and $6.68 \times 10^{-3} \text{ cm}^3 \text{ g}^{-1}$, respectively. Figure 2c shows BJH data of SD, SSD, and SDA biochars respectively, and Table 2 shows their surface characteristics.

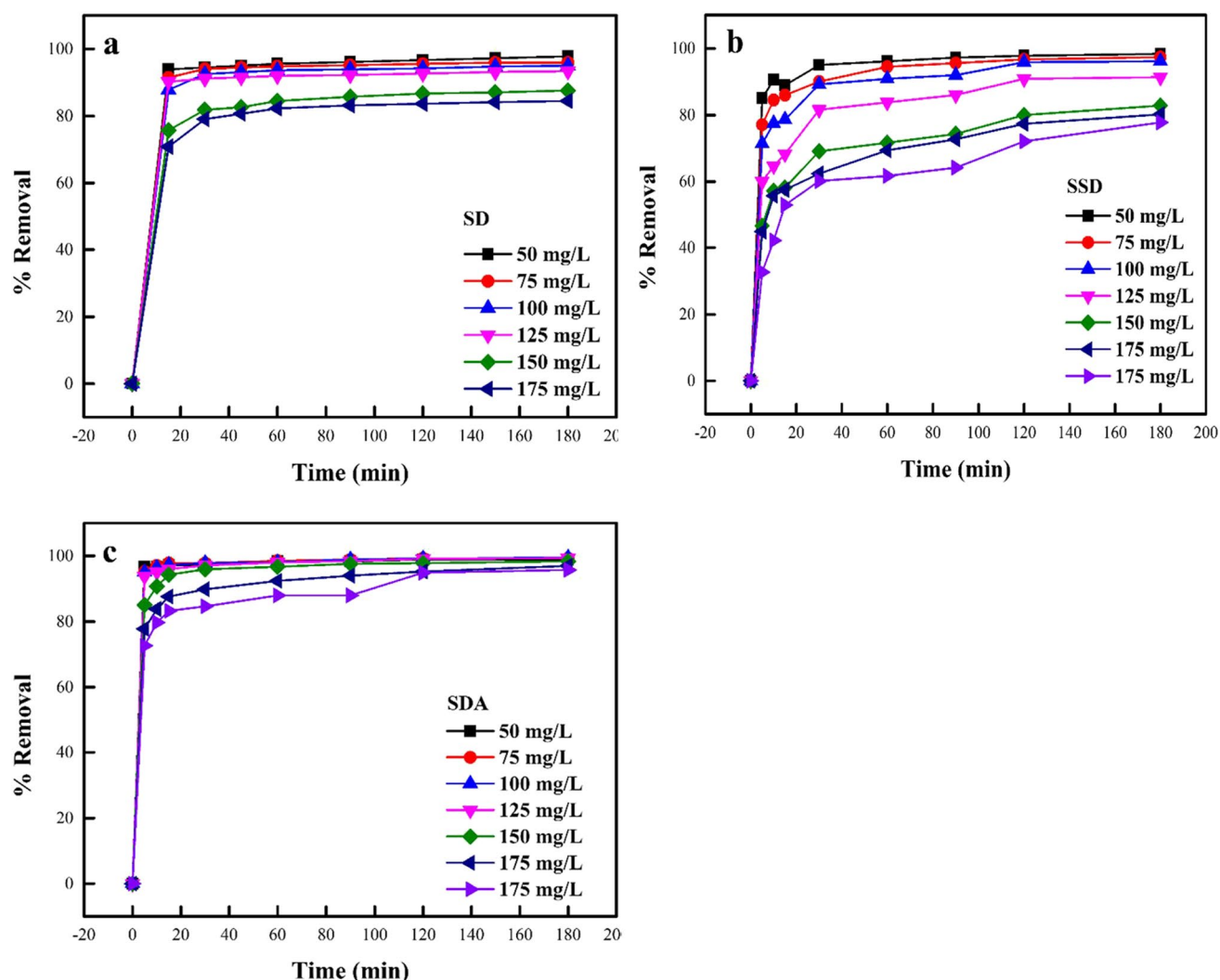


Fig. 7 Impact of interaction time on the confiscation of Cu(II) ions employing **a** SD, **b** SSD, and **c** SDA biochars

3.1.3 The morphological properties of the sawdust biochars surfaces

The surface morphology of sawdust raw material (RSD) and SD, SSD, and SDA biochars that was investigated using a scanning electron microscope (SEM) is shown in Fig. 3. As revealed in Fig. 3a and b, the SD and SSD biochars appear spotless and free of any particulate impurities. Besides, no impairment was noticed in the pores of the SSD as a result of sonications. Also, a small increase in the pore volume and the number of pores in SSD biochar due to sonication treatment of SD biochar were observed, which explains the small increase in the surface area of SSD biochar. Figure 3c shows the SDA biochar with a little pore occurring and reflects the minute surface area for SDA biochar. This proves our previous finding that the treatment of biochar with ammonium

solutions led to a decrease in the surface area due to pore blocking [58–60]. It is apparent that new-fangled pores of various sizes were produced in the SSD biochar as a result of sonication treatment; thus, the surface areas of the sonicated biochar increased while treatment with ammonium solutions led to pore blocking and subsequent decrease in the surface area of the produced SDA biochar. The SEM image of sawdust raw material represented in Fig. 3d showed no pores.

3.1.4 The elemental analysis of the sawdust biochars

The energy-dispersive X-ray spectrometer (EDX) was employed in analysing the chemical compositions of the sawdust biochar. The percentage (%) of elements in the SD, SSD, and SDA biochars was studied, and the results are described in Table 3, which illustrates the absence

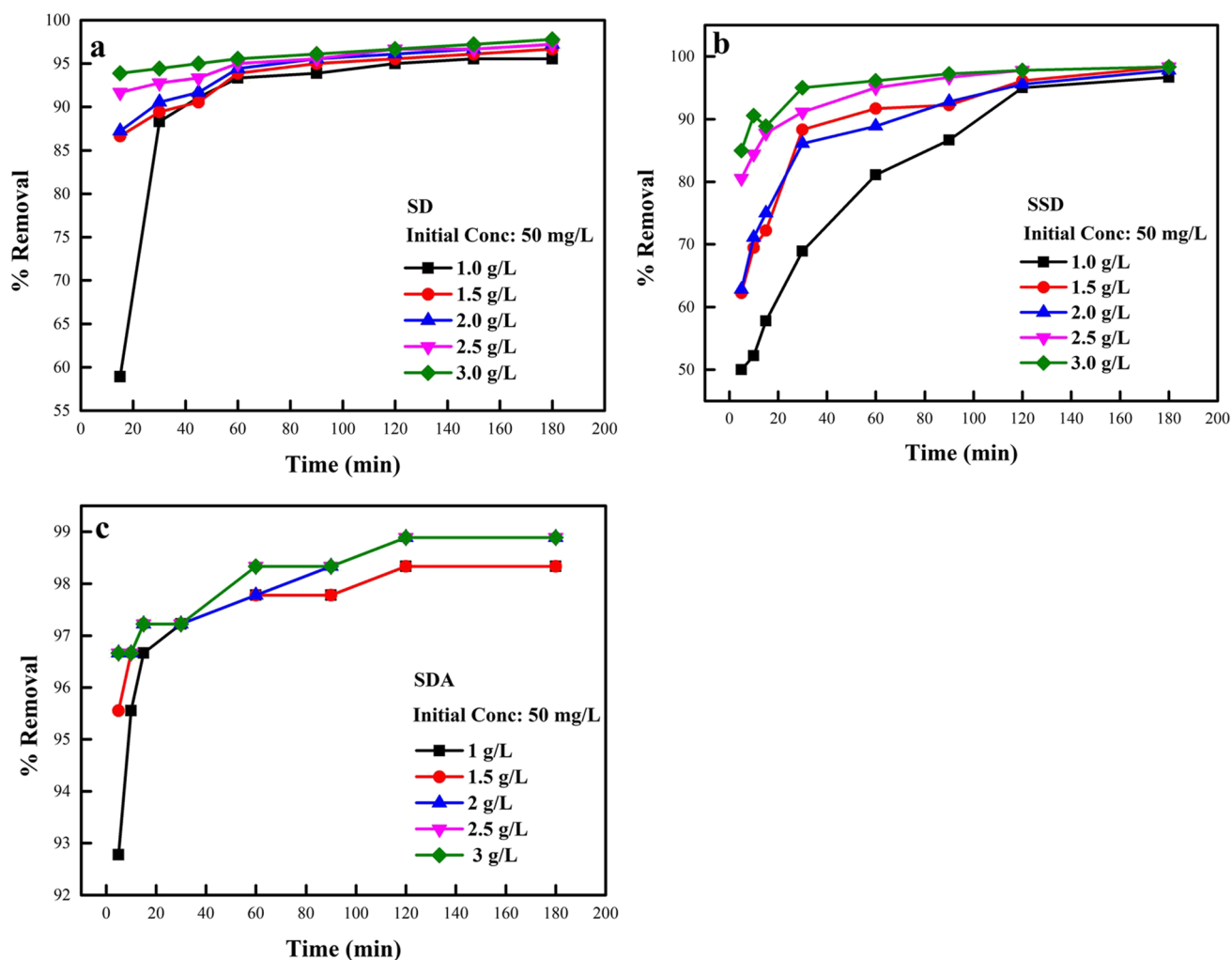


Fig. 8 Effect of biosorbent dose (1.0 g L^{-1}) on confiscations of Cu(II) using **a** SD, **b** SSD, and **c** SDA biochars

of an N_2 peak before the modifications with the NH_4OH reagent. The EDX analysis of SDA biochar verified the existence of approximately 7.63% N_2 of the sample weight.

3.1.5 Thermal characterizations of the biochars

In general, thermal gravimetric analysis (TGA) or thermogravimetric analysis means the measurement (quantifications) of the weight loss during a user-distinct temperature or heating procedure. Figure 4a and b show the decompositions of SD and SSD biochars, respectively, which occur in 3 stages (phases), while the decompositions of the SDA biochar take place in 4 phases (Fig. 5c). In SD biochar, the first step of decompositions ensues

at a temperature range between 50 and 150 °C, which encompasses the loss of surface-bound water and moisture existing in the sample with a weight loss of around 6.76%; the second step, temperatures ranging from 150 to 700 °C and approximate weight loss 56.30%; and in the third decomposition step, temperatures ranging from 700 to 1000 °C and approximate weight loss 22.55%. In SSD biochar, the first step of decompositions occurs at temperatures ranging from 50 to 180 °C, with an approximate weight loss of 12.21%; the second step, temperatures ranging from 180 to 675 °C and approximate weight loss of 32.31%; and in the third decomposition step, temperatures ranging from 675 to 1000 °C and approximate weight loss 4.28%, while in SDA biochar, the first step of decompositions ensues at temperatures ranging from

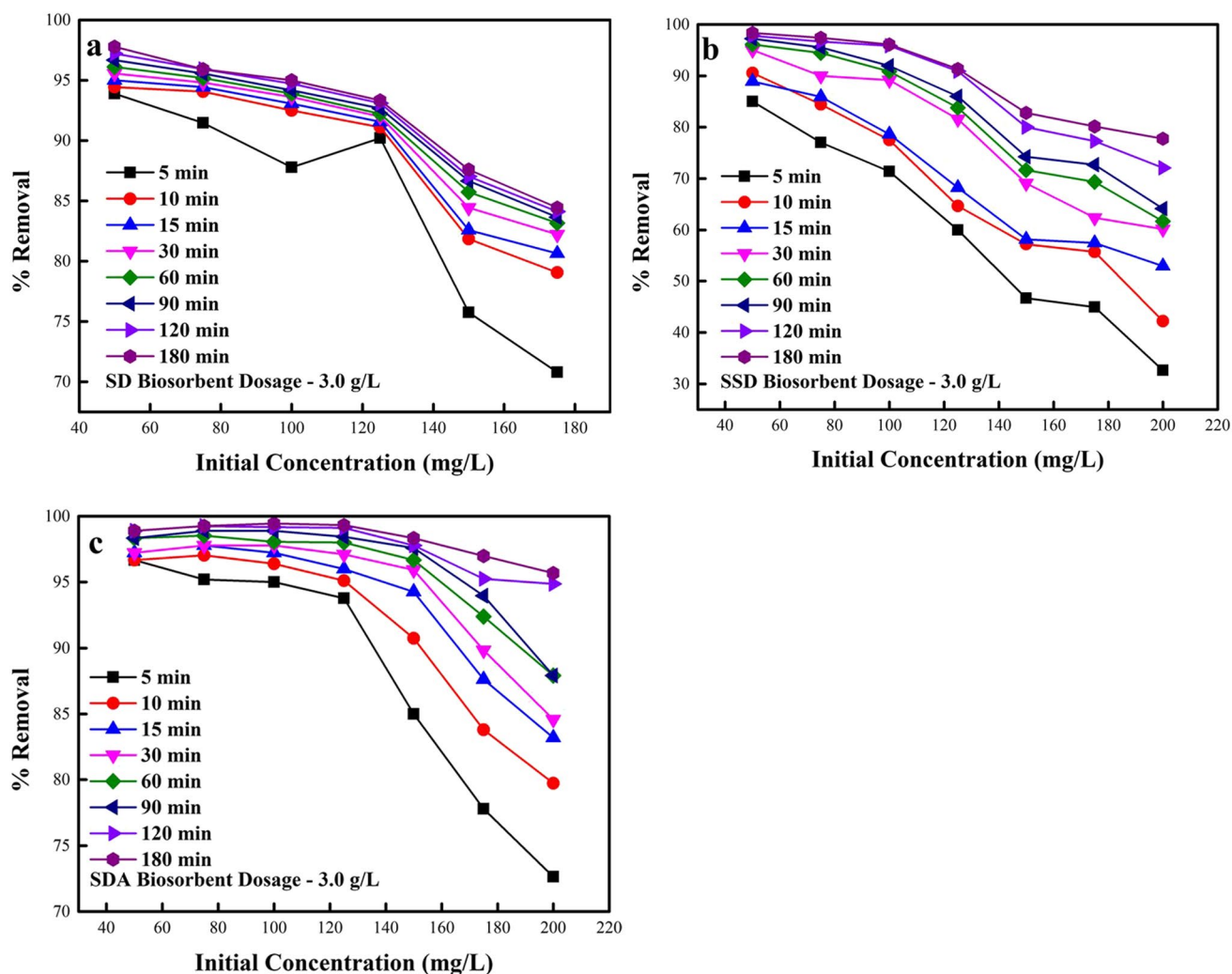


Fig. 9 Effect of initial conc of Cu(II) (3.0 g L^{-1}) on its confiscations. **a** SD, **b** SSD, and **c** SDA biochars

50 to 180 °C, which involves approximately weight loss of 13.21%; the second step, temperatures ranging from 180 to 250 °C and approximate weight loss of 3.99%; in the third decomposition step, temperatures ranging from 250 to 700 °C and approximate weight loss of 30.08%; and in the fourth step, temperatures ranging from 700 to 1000 °C and approximate weight loss of 2.96%.

3.1.6 XRD analysis of SD, SSD, and SDA biochars

Figure 5 shows the XRD of the SD, SDA, and SSD biochars. The broad peak in the region of $2\theta = 10\text{--}30$ is indexed as C (002) diffraction peak indicating an amorphous carbon structure with randomly oriented aromatic sheets. For SD, SSD, and SDA biochars, there are sharp

peaks around $2\theta = 43.65$, while, in the case of SDA, there are more two sharp peaks around $2\theta = 25.8$ and 63.9 , which correspond to the miscellaneous inorganic components mainly constituted of quartz and albite, within the structure of SD biochar [61, 62].

3.2 Effect of solutions pH on the removal of Cu(II) ions

A critical parameter that decides the sequestration level in the biosorption process is the solution's pH. This impacts the biosorbent surface charge and the degree of ionization. The biosorption dependence on the pH is described based on the FGs' participation in the uptake of metal ions and their chemistry [22, 28]. The impact

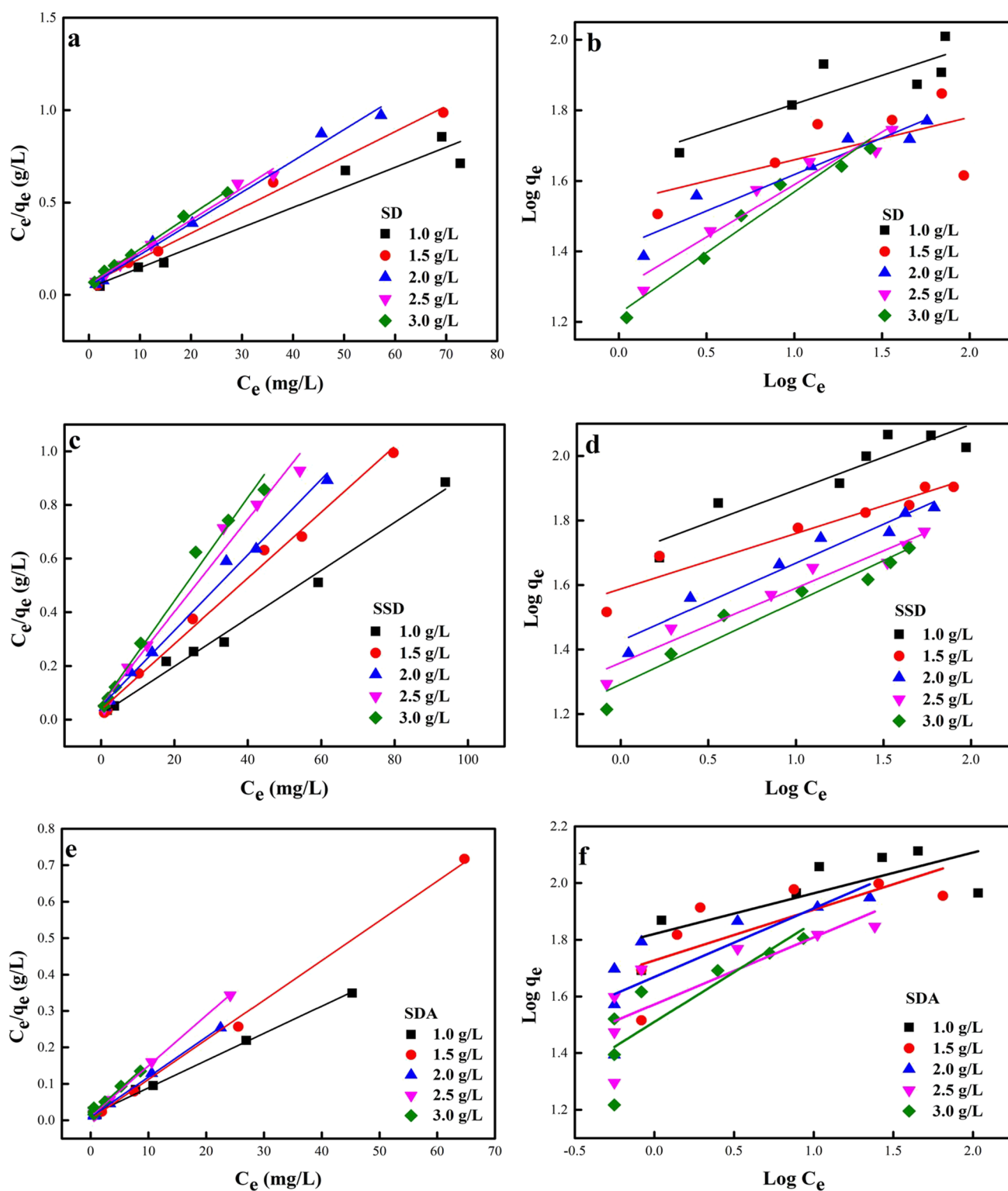


Fig. 10 Linear plots of experimental data using **a** LNR model and **b** FRD model using SD biochar, **c** LNR model and **d** FRD model using SSD biochar, **e** LNR model and **f** FRD model using SDA biochar, and Temkin model using **g** SD biochar, **h** SSD biochar, and **i** SDA biochar

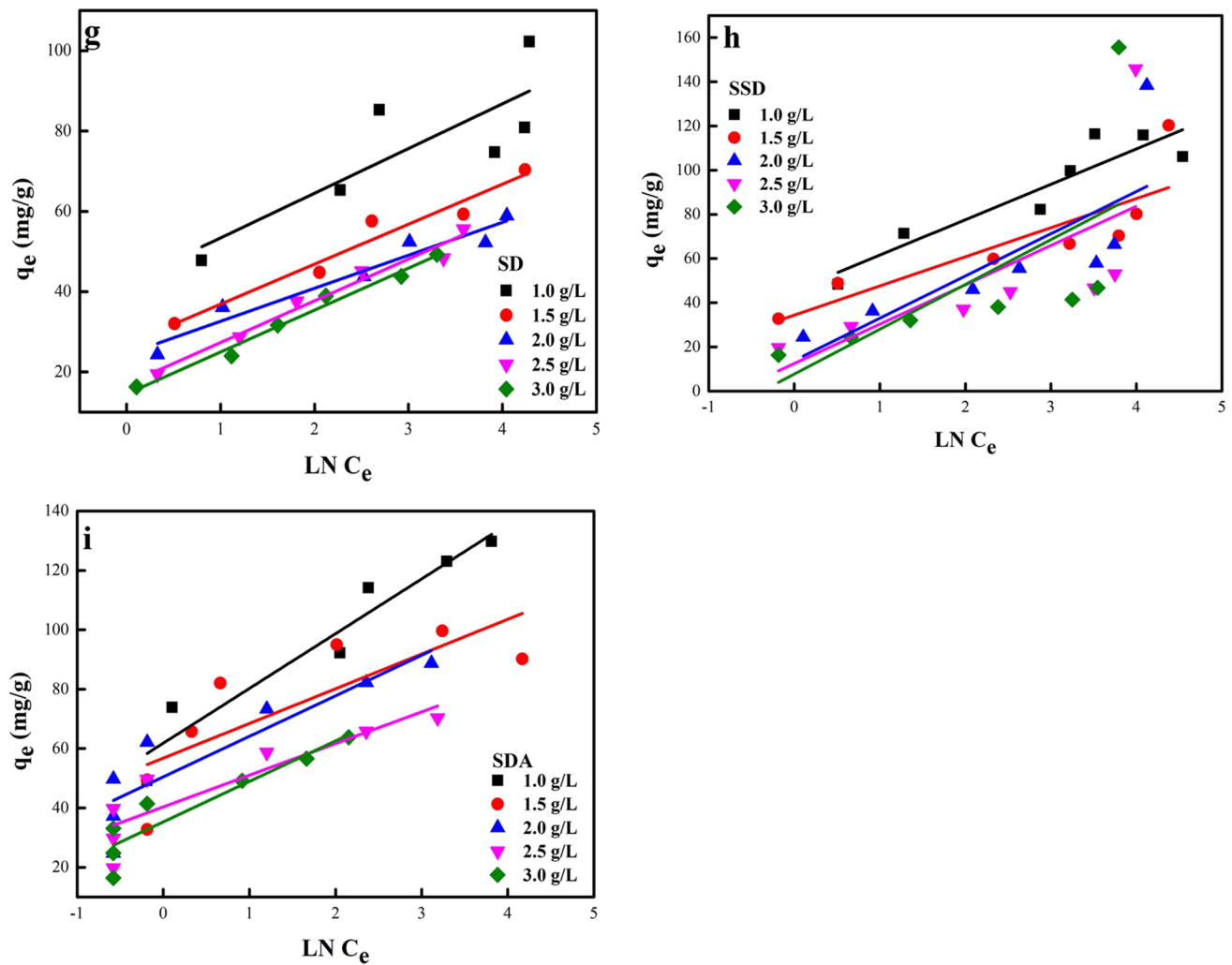


Fig. 10 (continued)

Table 4 Calculated variables from the biosorption of Cu(II) ions onto SD, SSD, and SDA biochars employing LNR and FRD models

Biochar		LNR model			FRH model		
Type	Dose	Q_m	K_L	R^2	n	K_F	R^2
SD	1.0	91.74	289.12	0.9562	1.627	45.175	0.7399
	1.5	46.95	− 317.91	0.9064	0.1205	34.61	0.4037
	2.0	58.82	361.7	0.9922	0.2073	25.734	0.9125
	2.5	57.8	301.39	0.9911	0.2982	19.543	0.7433
	3.0	54.05	296	0.9955	0.3452	16.726	0.9655
SSD	1.0	112.36	447.24	0.991	0.203	49.147	0.8678
	1.5	81.30	336.07	0.993	0.172	38.672	0.9250
	2.0	70.92	279.76	0.992	0.241	26.712	0.9529
	2.5	57.80	306.74	0.985	0.231	22.845	0.9538
	3.0	52.08	333.91	0.986	0.255	19.597	0.9470
SDA	1.0	133.33	524.48	0.997	0.144	66.176	0.5970
	1.5	91.74	3516.13	0.998	0.179	53.395	0.5775
	2.0	91.74	1184.78	0.998	0.242	46.666	0.6579
	2.5	72.46	1232.14	0.998	0.237	37.325	0.6508
	3.0	70.42	946.67	0.982	0.351	32.359	0.7202

Table 5 Calculated parameters from the biosorption of Cu(II) onto SD, SSD, and SDA biochars using Temkin model

Isotherm Model	Isotherm Parameters	Dosage				
		1 g L ⁻¹	1.5 g L ⁻¹	2.0 g L ⁻¹	2.5 g L ⁻¹	3.0 g L ⁻¹
Temkin (SD)	$A_T (L g^{-1})$	44.61	14.61	19.48	5.10	4.03
	$B (J mol^{-1})$	11.13	9.96	8.22	10.39	10.44
	R^2	0.609	0.937	0.930	0.966	0.981
Temkin (SSD)	$A_T (L g^{-1})$	28.57	128.44	39.85	43.65	13.33
	$B (J mol^{-1})$	18.44	11.69	13.69	10.68	13.63
	R^2	0.833	0.676	0.529	0.350	0.319
Temkin (SDA)	$A_T (L g^{-1})$	17.13	13.54	2.07	2.02	1.47
	$B (J mol^{-1})$	16.03	13.20	19.13	17.80	20.27
	R^2	0.918	0.585	0.766	0.757	0.837

Table 6 Comparison of reported sorption capacities of different biosorbents for Cu(II) removal

Biosorbents	Q_m (mg g ⁻¹)	References
Dragon fruit peel (DFP), rambutan peel (RP), and passions fruit peel (PFP)	92.59, 192.31, and 121.95	[28]
Pre-boiled wood chips (BWC), formaldehyde-treated wood chips (FWC), and sulfuric acid-treated wood chips (SWC)	15.53, 15.53, and 16.86	[63]
Alginate/montmorillonite and alginate/kaolin	0.44 ± 0.03 and 0.27 ± 0.08	[72]
Mineral-rich biochar derived from a spent <i>Agaricus bisporus</i> substrate (SAS)	68.10, 55.20, and 64.80	[79]
<i>Humulus scandens</i> biochars	221.00	[80]
Muskmelon peel biochar	79.36	[81]
<i>Chaenomeles sinensis</i> seed biochar	105.12	[82]
SD, SSD, and SDA	91.74, 112.36, and 133.33	This study

of pH on Cu(II) ion removal efficiency was considered with changing pH values from pH 1 to 5. The point of zero charge (pH_{PZC}) of the synthesized biochars (SD, SSD, and SDA) was determined to be 4.4, 4.7, and 4.9 (Fig. 6a), which denotes that the biosorbent surface was positively charged when $pH < pH_{PZC}$ and negatively charged when $pH > pH_{PZC}$. In a water-soluble solution, Cu occurs as Cu^{2+} , $Cu(OH)_2$, and $Cu(OH)^+$ and, at low solution pH (pH 2 and 5.5), the predominant species in water-soluble solutions are $Cu(OH)^+$ and Cu^{2+} [63]. Figure 6b shows the removal % of Cu(II) ions onto the various biosorbents, and it was noticed that the percentage of Cu(II) ions removed increased with rising pH values with optimum confiscations noticed at pH 5.8 (SD: 69%, SSD: 74%, and SDA: 77%). At lower pH values, the biosorbent surface was protonated with surplus H^+ , leading to the accessible active sites on the biosorbent surface being positively charged and hence sturdy electrostatic repulsions for Cu(II) ions. With an additional rise in the solution's pH, the accessible surface charge on the biosorbent surface was deprotonated and hence

negatively charged. This led to the electrostatic attraction between Cu(II) ions and the negatively charged active sites on the biosorbent. At pH values of 6 and above, Cu was reported to precipitate to $Cu(OH)_2$ and hydrolysis was also reported to occur, thereby creating a colloidal compound [22, 64]. The modified SDA and SSD biochars were noticed to have improved sorptions for Cu(II) ions in comparison to SD biochar owing to the increased surface area and huge pore size leading to an increase in the available sorption sites for Cu(II) ion removal. Further biosorption investigations were undertaken at pH 5.5–6.0 [28, 65, 66].

3.3 Effect of contact time on Cu(II) ion adsorption

Figure 7 shows the increase in the percentage of Cu(II) ions confiscated to SD, SSD, and SDA biochars as the contact time of the interactions between the sorbate and biochars was increased from 0 to 180 min, with equilibrium being attained at 60 and 120 min for SD and SSD and SDA biochars. The rapid biosorption process

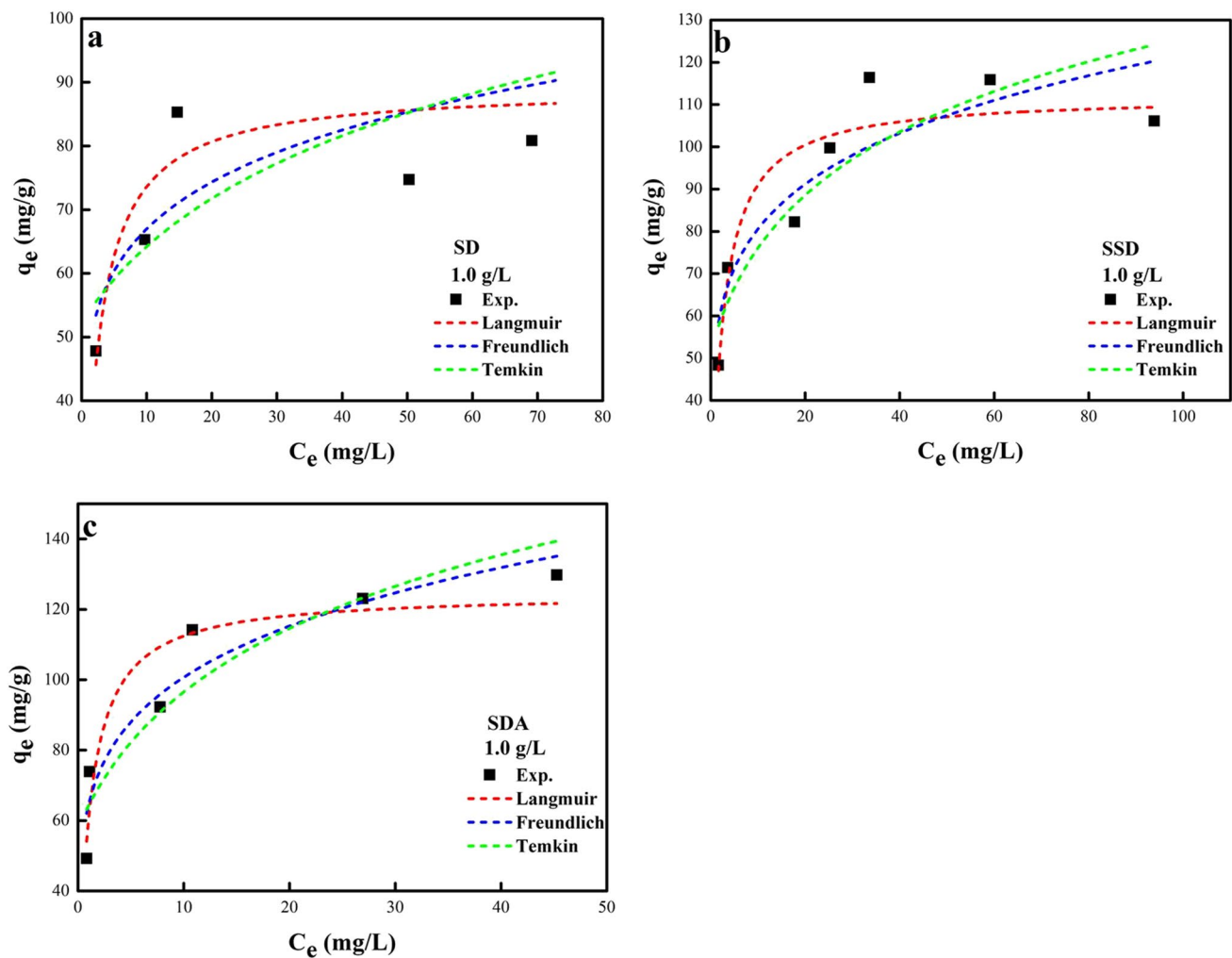


Fig. 11 Non-linear plot of LNR, FRH, and Temkin models

followed by the subsequent equilibrium trend attained was attributed to the available accessible vacant sites at the initial stage of the biosorption process leading to momentous biosorption rate and the saturations or occupations of accessible vacant sites as the treatment time was enhanced, thereby resulting in reduced biosorption rate [22, 67].

3.4 Effect of biochar dosage on the adsorption of Cu(II) ions

Biosorbent dosage optimizations are one of the crucial factors that limit the biosorbent sorptions capacity at various working settings, and it is essential in determining the least amount needed for optimum sorptions to be attained.

The biosorption of Cu(II) ions was evaluated by changing biosorbent dosage using SD, SSD, and SDA biochars while keeping other parameters constants. As noticed in Fig. 8, the percentage of Cu(II) ions removed using the various biochars increased with increasing biosorbent dosage employed, with an optimum removal % of 98.89%, 98.33% achieved using SDA, SSD, and SD biosorbent dosage of 1 g L^{-1} , respectively. This trend of increasing biosorbent dosage leading to enhancing % of Cu(II) ions confiscated was ascribed to increased active accessible sites available coupled with elevated surface area as the biosorbent dosage was improved, leading to enhanced biosorption of Cu(II) ions [22]. A similar inclination of improved % of Cu(II) ions removed using different biosorbents was also reported in the study by [68–70].

Table 7 Calculated variables from the biosorption of Cu(II) ions onto SD, SSD, and SDA biochars employing non-linear LNR, FRD, and Temkin models

Biochar	Dose	LNR model			FRH model			Temkin model		
		Q_m /standard error	K_L /standard error	R^2	Chi-sqr	n/standard error	K_F /standard error	R^2	Chi-sqr	A /standard error
SD	1.0	89.21/7.04515	0.4717/0.25178	0.6246	128.41274	6.65/2.61569	47.38/10.05475	0.5825	142.79203	20.5959/2.07227
SSD		112.04952/5.90389	0.43341/0.13705	0.83944	102.93095	5.59171/1.33877	53.37031/8.1483	0.78638	136.95164	26.91436/1.762
SDA		124.58012/7.23322	0.92623/0.2824	0.86929	127.8205	5.13755/0.88767	64.31707/6.30733	0.89304	104.59577	35.57483/2.36176
										B /standard error
										12.59747/10.06482
										6.86054/3.71808
										5.07066/1.7902
										R^2
										0.50433
										0.74199
										165.40974
										155.57738

3.5 Effect of initial concentrations on Cu(II) ion confiscations

To determine the impact of varying initial conc (50–200 mg L⁻¹) on the sequestrations of Cu(II) ions, experiments were operated at an ambient temperature, contact time of 5–180 min, and pH 5. Results shown in Fig. 9 show the extent of removal % as a function of Cu(II) ion initial conc. It was noticed that the extent of Cu(II) ion removal % reduced with increasing Cu(II) ion conc (optimum removal: SD: 97.8–93.8%, SSD: 98.3–85.0%, and SDA: 98.9–96.7%). At low conc of Cu(II) ions, decreased removal with increasing initial conc was ascribed to the elevated driving force in terms of biosorbents binding sites accessible and available, whereas the increased struggle for limited sorptions sites at elevated conc led to reduced removal of Cu(II) ions and thus more Cu(II) ions are left unabsorbed in the solutions due to the rapid saturations of sorptions sites. These assertions reported in this study are also supported by the study of Gupta et al. [22], Larous and Meniai [64], Eldeeb et al. [67], Yu et al. [71], and Răpă et al. [72].

3.6 Biosorption isotherms

The sorption isotherm is essential and of functional significance, as it shows the systematic sorptions features (monolayer against multi-layer), heterogeneity of a surface, and the sorbate and sorbent interactions. It also provides information on the loading sorbent capacity for functional purposes [73]. The sorption capacities of the studied biosorbents were evaluated by corresponding equilibrium isotherm model constructions employing Langmuir (LNR), Freundlich (FRH), and Temkin models [74].

The sorption process that relates to a comprehensive uniform surface with trivial interactions between sorbed molecules defines the LNR models [71]. In the descriptions of the sorptions of noxious metal ions, the LNR model is generally employed as it explains the quantifiable monolayer sorbate structure on the biosorbent surface and, after the formations of the monolayer sorbate structure, no additional biosorption process takes place, while the FRH defines the changeable heterogeneous sorptions without limiting the sorption process to a particular monolayer. It forecasts that the conc of sorbate on the sorbent will improve without permeations according to the improved conc of the sorbate in the liquid solutions [75]. The Temkin model assumes that the heat of the adsorption reduces linearly with coverage (multi-layer process), owing to the interaction between the

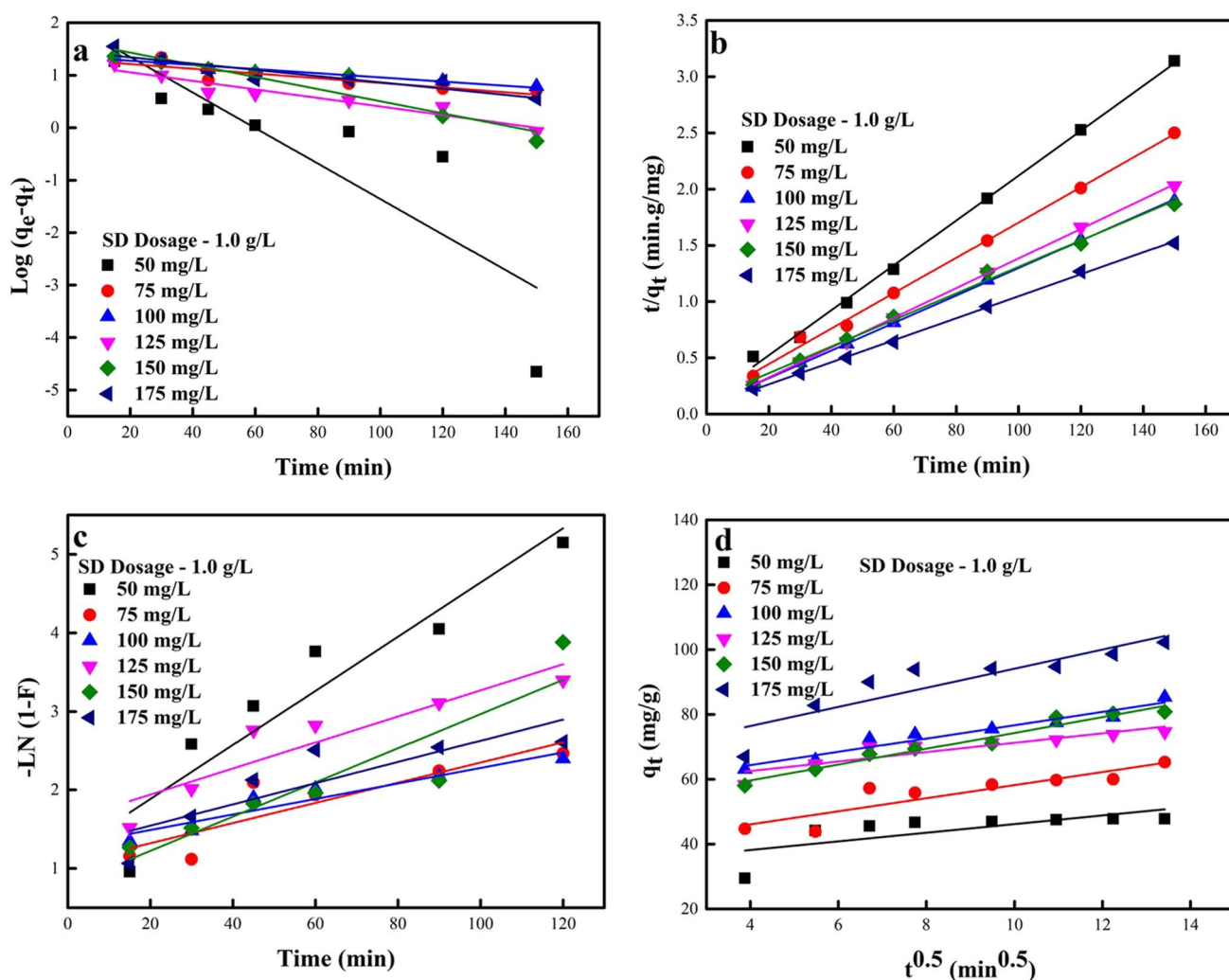


Fig. 12 Linear plots of experimental data using **a** PFO model, **b** PSO model, **c** FD model, and **d** IPD model using SD biochar

adsorbent and adsorbate and the adsorption is described by the steady binding energy distribution [76–78].

The linear plots of the LNR, FRH, and Temkin models and their fitting results are shown in Fig. 10 employing SD, SSD, and SDA biochars. The R^2 values of the LNR model ($R^2 > 0.9$) were noticed to have superior values to those of the FRH and Temkin models, which was indicative of the sorption process of Cu(II) ions to biochars best defined using the linearized LNR model and with the biosorption of Cu(II) ions forming a monolayer onto the active sites on the surface of the biochars (Tables 4 and 5). The determined optimum sorption capacities (Q_m) employing the LNR model for Cu(II) ion confiscations to SD, SSD, and SDA biochars were 91.74, 112.36, and 133.33 mg g^{-1} , respectively. The Q_m values of SDA were to some extent greater than those of SSD and SD owing

to the possible higher main FGs in the structure of SDA biochar. Hence, SDA biochar had extra binding active spots and more negative surfaces, thus improving Cu(II) ion retentions on the surface of SDA biochar. A comparison of the optimum monolayer sorption capacities of SD, SSD, and SDA biochars with other reported biosorbents shows that the biochars employed in this study for Cu(II) ion removal were superior to other biosorbents (Table 6). Table 6 contains the comparison of reported sorption capacities of different biosorbents for Cu(II) removal.

For linear regression, altering the unique equation can contravene the theories currently behind the model; thereby, parameter estimation gives the ideal fitting parameters for the linear form of the model and not for the original non-linear model (Fig. 11). To approximate models' parameters, the non-linear regression is

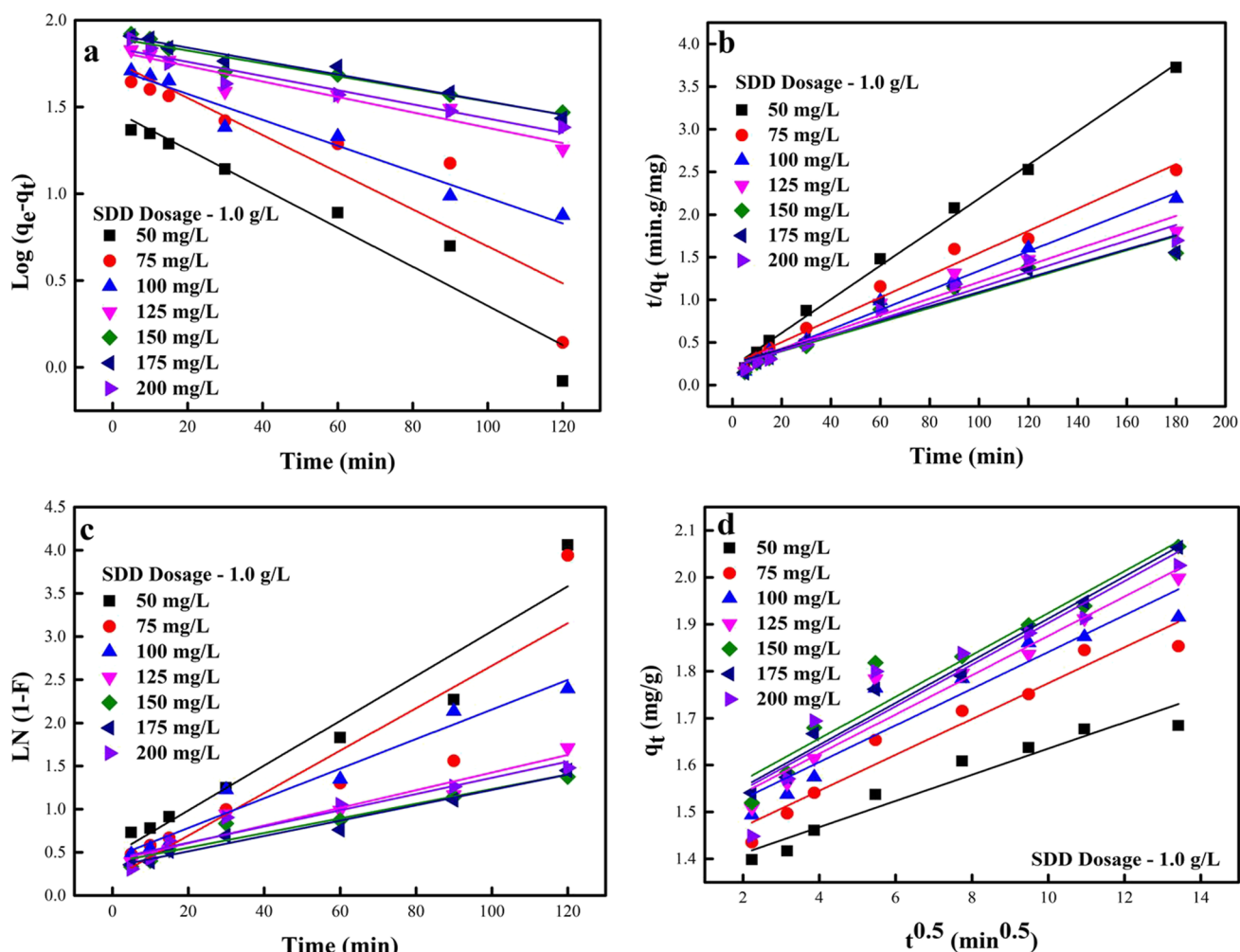


Fig. 13 Linear plots of experimental data using **a** PFO model, **b** PSO model, **c** FD model, and **d** IPD model using SSD biochar

the conventional technique employed and it is utilized when the isotherm model cannot be linearized. Comparing these two techniques, the non-linear regression is a more practical technique that can be utilized to assess isotherm model parameters [83]. The precision of the non-linear isotherm models fit to experimental data was evaluated using error functions calculation such as coefficient of determination (R^2) and chi-square (χ^2), which are statistical equations employed to measure the deviation of the theoretically predicted data from the actual values of the experimental data. The ideal model is one with the lowest χ^2 and R^2 value that is close to unity. R^2 signifies the percentage of flexibility in the dependent variable and its values range between 0 and 1. When the calculated value is comparable to the experimental values, χ^2 is close to zero, while an elevated value of χ^2 shows a high bias between the calculated model and

experimental values [84]. To describe the biosorption of Cu(II) onto SD, SSD, and SDA biochars, the non-linear regression analysis of the three isotherm models was explored (Table 7). The χ^2 and R^2 were considered for non-linear regression analysis, and from the results presented in Table 7, χ^2 values obtained for each model using SD, SSD, and SDA show that the fitting degree was in the following sequence: LNR (ideal fit) > FRH > Temkin (SD and SSD) and FRH (ideal fit) > LNR > Temkin (SDA). Comparing the R^2 values obtained in Table 7 for the isotherm models considered, the degree of fitting was in the order of LNR (ideal fit) > FRH > Temkin (SD and SSD) and FRH (ideal fit) > LNR > Temkin (SDA). As noticed from the values obtained, LNR and FRH ideally described the biosorption of Cu(II) ions to SD and SSD and SDA owing to the low values of χ^2 and R^2 obtained when compared to other isotherm models.

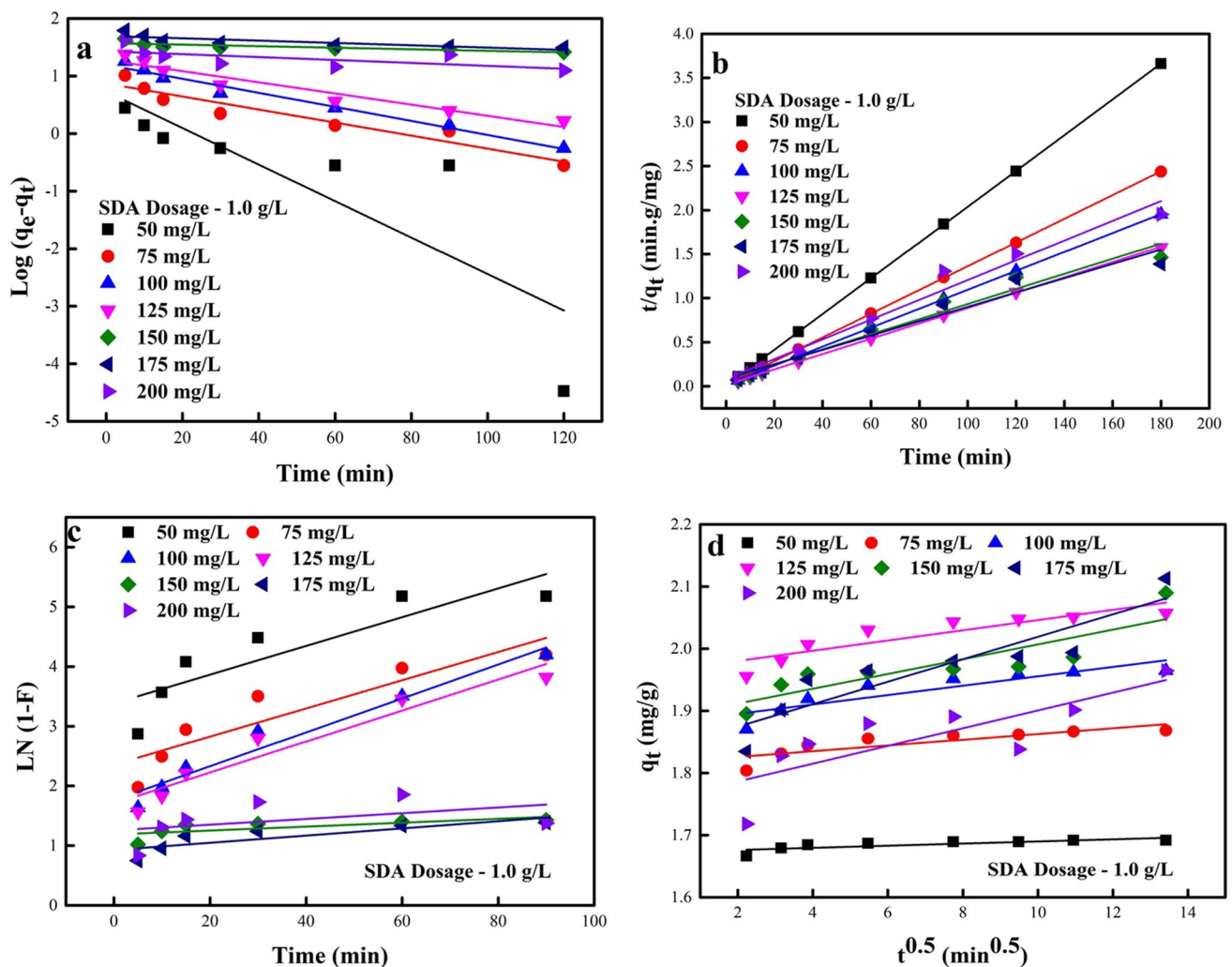


Fig. 14 Linear plots of experimental data using **a** PFO model, **b** PSO model, **c** FD model, and **d** IPD model with SDA biochar

3.7 Biosorption kinetics

A key parameter that characterizes the sorption effectiveness is the sorption kinetic model, and it is a critical feature in sorption system design to approximate the sorption process rate for specific systems. To evaluate the intricate mechanisms and the design of huge scale sorption systems in the time to come, the sorption kinetic models are employed. Sorption trends can be regulated by various pollutants transfer mechanisms from the solutions to the biosorbent. Hence, the resulting circumstances involved for metal retentions to occur like the metal diffusions from the solutions to the biosorbent surface contact area, surface diffusions to the pores and metal complexations, physicochemical sorptions, or

chemisorptions are established by kinetic models [85]. To ascertain the optimum operation conditions, which is critical for a full-scale batch procedure, the kinetics of the biosorption of Cu(II) ions onto SD, SSD, and SDA were explored using the pseudo-first-order (PFO) model, pseudo-second-order (PSO) model, film diffusion (FD), and intraparticle diffusion (IPD). The linear plots of these models and experimental data comparison using the various biochars are shown in Figs. 12, 13 and 14 and Tables 8, 9, 10, 11, 12 and 13. From the calculated parameters depicted in Tables 8, 9, 10, 11, 12 and 13, it was noticed that the PSO model equations fitted better than other models to the experimental data, with a coefficient of regressions ($R^2 > 0.92$) using SD, SSD, and SDA biochars, which was suggestive of the biosorption

Table 8 Calculated parameters of the confiscations of Cu(II) to SD biochar employing the PFO and PSO models

Parameter			PFO model				PSO model			
SD conc	Cu, mg L ⁻¹	<i>q</i> _e (exp.)	<i>q</i> _e (calc.)	<i>k</i> ₁ × 10 ³	<i>R</i> ²	<i>q</i> _e (calc.)	<i>k</i> ² × 10 ³	<i>h</i>	<i>R</i> ²	
1.0 g L ⁻¹	50	47.78	139.798	83.1383	0.840	49.50	21.80	53,435.29	0.999	
	75	65.28	311.602	55.5023	0.508	66.67	25.96	115,380.18	0.994	
	100	85.28	269.96	55.5023	0.496	86.21	68.75	510,907.58	0.995	
	125	74.72	16.508	18.6543	0.919	76.34	86.33	503,049.87	1.000	
	150	80.83	46.057	26.7148	0.907	85.47	55.26	403,668.72	0.997	
	175	102.22	28.907	13.818	0.849	105.26	134.63	1,491,783.31	0.998	
1.5 g L ⁻¹	50	32.04	4.414	21.4179	0.933	32.68	12.59	13,449.88	1.000	
	75	44.81	9.447	22.7997	0.957	45.87	22.17	46,656.03	1.000	
	100	57.59	174.141	59.1871	0.609	58.48	25.85	88,400.70	0.996	
	125	59.26	61.277	50.666	0.552	59.88	55.16	197,797.48	1.000	
	150	41.23	46.548	57.3447	0.734	42.19	19.23	34,229.11	1.000	
	175	70.37	129.003	55.0417	0.570	71.94	63.04	326,285.40	0.999	
2.0 g L ⁻¹	50	24.31	14.0185	49.0539	0.677	24.63	5.73	3475.36	1.000	
	75	36.11	5.152	10.5938	0.641	36.36	11.17	14,767.86	0.999	
	100	43.75	5.394	12.8968	0.952	44.05	26.08	50,620.17	1.000	
	125	52.36	8.1077	22.1088	0.979	53.19	50.08	141,683.79	1.000	
	150	52.22	13.8388	28.5572	0.971	53.48	36.34	103,910.36	1.000	
	175	58.89	69.422	56.6538	0.577	59.52	64.30	227,830.19	1.000	
2.5 g L ⁻¹	50	19.44	1.549	18.8846	0.955	19.57	4.36	1668.51	1.000	
	75	28.67	15.911	69.7809	0.848	28.99	16.31	13,706.18	1.000	
	100	37.56	17.486	48.1327	0.621	37.88	26.77	38,407.81	1.000	
	125	45.11	4.078	10.5938	0.713	45.25	36.76	75,261.99	1.000	
	150	48.33	7.223	24.8724	0.974	49.02	43.77	105,173.66	1.000	
	175	55.56	36.091	52.5084	0.660	56.50	64.22	204,998.44	1.000	
3.0 g L ⁻¹	50	16.30	6.331	51.3569	0.562	16.37	3.28	879.32	1.000	
	75	23.98	10.228	68.6294	0.799	24.10	15.69	9111.84	1.000	
	100	31.67	8.978	47.9024	0.655	31.85	25.61	25,976.83	1.000	
	125	38.89	10.184	50.8963	0.611	39.06	62.79	95,815.08	1.000	
	150	43.80	54.815	61.4901	0.621	44.44	29.75	58,762.71	1.000	
	175	49.26	36.534	54.1205	0.703	50.00	44.40	111,012.43	1.000	

of Cu(II) ions to the various biochars that were measured by chemical biosorption mechanism and the sorption rate was linked to the biosorption active sites on the surface of the biochar [82]. These results show that the biosorption of Cu(II) to the biochars was a rate-limiting step that has valence force between the biochars and the sorbate, with electron exchange or sharing [28]. Răpă et al. [72] equally found in their biosorption of Cu(II) ions to alginate/clay hybrid composite beads study that the PSO model best described the biosorption process [72]. While in the studies of Bai et al. [80], Hu et al. [82], and Khan et al. [81] where *Humulus scandens*-derived biochar, biochar derived from *Chaenomeles sinensis* seed, and muskmelon peel biochar were utilized for the biosorption of Cu(II) ions, it was noticed that the biosorption

processes were best close-fitting to the experimental data using the PSO model [86–93]. While in the studies of Sachan and Das [86] and Rahim et al. [87] where the biosorption of Cu(II) ions to biochar obtained from plant biomass *Saccarum ravvane* and decorated with manganese dioxide and desiccated coconut waste (DCW) effectiveness was assessed, it was noticed that the biosorption process followed the PSO model.

3.8 Optimization study

The design matrix was employed for investigating the interactions effects of three significant factors, including the contact time, SD biochar dose, and initial Cu(II) ion conc on the percentage of removal of Cu(II) ions. The

Table 9 Calculated parameters of the confiscations of Cu(II) ions to SSD biochar employing the PFO and PSO models

Parameter			PFO model				PSO model			
SSD conc	Cu, mg L ⁻¹	<i>q_e</i> (exp.)	<i>q_e</i> (calc.)	<i>k</i> ₁ ×10 ³	<i>R</i> ²	<i>q_e</i> (calc.)	<i>k</i> ² ×10 ³	<i>h</i>	<i>R</i> ²	
1.0 g L ⁻¹	50	48.33	30. +E7	26.02	0.932	50.76	11.95	30,781.16	0.997	
	75	32.78	211.59	61.95	0.774	76.34	24.17	140,837.27	0.983	
	100	24.44	53.10	17.27	0.962	87.72	39.62	304,881.71	0.992	
	125	19.67	66.82	10.13	0.930	103.09	45.42	482,722.13	0.956	
	150	16.39	460.05	59.42	0.640	117.65	60.92	843,171.60	0.940	
	175	71.39	65.96	8.98	0.973	119.05	55.73	789,835.22	0.925	
	200	48.89	69.53	9.44	0.924	108.70	54.65	645,643.82	0.962	
1.5 g L ⁻¹	50	36.25	45.60	51.13	0.798	33.33	7.68	8537.81	0.999	
	75	28.22	61.67	56.88	0.788	50.00	21.11	52,787.16	1.000	
	100	24.35	108.22	55.50	0.743	61.73	23.68	90,236.84	0.996	
	125	82.22	168.42	52.05	0.660	66.67	15.51	68,946.20	0.946	
	150	59.82	39.17	14.05	0.821	71.94	25.28	130,864.83	0.972	
	175	45.97	58.25	18.42	0.856	80.65	33.40	217,243.76	0.973	
	200	37.11	60.90	18.42	0.842	80.65	31.03	201,800.40	0.969	
2.0 g L ⁻¹	50	32.04	8.01	21.88	0.969	24.88	3.23	1998.48	0.999	
	75	99.72	13.04	21.42	0.963	36.90	9.17	12,485.23	0.999	
	100	66.67	21.95	20.27	0.939	47.39	12.33	27,705.13	0.997	
	125	55.56	93.41	50.67	0.727	56.82	16.57	53,500.81	0.990	
	150	45.00	106.02	53.43	0.755	59.88	18.55	66,512.35	0.994	
	175	38.06	160.33	56.88	0.683	67.57	23.61	107,769.70	0.990	
	200	116.39	36.79	10.82	0.845	69.44	22.38	107,919.90	0.971	
2.5 g L ⁻¹	50	70.37	6.76	46.29	0.896	19.84	3.88	1528.41	1.000	
	75	57.92	8.68	29.48	0.975	29.76	7.57	6705.90	1.000	
	100	46.67	14.15	23.26	0.890	37.88	9.60	13,779.51	0.998	
	125	41.39	23.42	25.10	0.841	46.30	11.86	25,423.00	0.995	
	150	115.83	67.44	51.59	0.756	47.62	12.15	27,555.68	0.993	
	175	80.19	27.68	20.50	0.878	54.64	16.57	49,481.27	0.993	
	200	66.39	30.25	12.44	0.826	58.82	15.17	52,490.26	0.976	
3.0 g L ⁻¹	50	53.00	3.97	47.67	0.860	16.47	3.52	955.41	1.000	
	75	46.76	10.17	50.21	0.856	24.57	7.09	4282.45	1.000	
	100	106.11	9.39	32.24	0.871	32.47	11.05	11,647.93	1.000	
	125	120.28	31.73	51.82	0.877	38.91	12.15	18,397.10	0.999	
	150	1387.33	57.40	55.27	0.749	42.19	10.93	19,457.43	0.998	
	175	145.83	19.32	19.11	0.972	47.85	15.08	34,525.75	0.998	
	200	155.56	27.40	17.04	0.946	52.91	13.62	38,136.46	0.992	

design of the experiment and the responses are reported in Table 14. As a result of the obtained results, the following polynomial equations for Cu(II) ion removal using SD biochar were established for the removal % for coded factors (CF) and actual factors (AF) from Eqs. (5) and (6), and using SSD biochar, Eqs. (7) and (8) were used to develop the removal % for CF and AF. The polynomial equations for Cu(II) ion removal using SDA biochar were developed for removal % for CF and AF using Eqs. (9) and (10).

$$\begin{aligned} \text{Removal \% for CF} = & 82.31 + 10.39A - 14.25B + 5.92C + 6.47AB - 2.76AC \\ & + 1.06BC + 0.4388A^2 - 0.4799B^2 - 4.11C^2 \end{aligned} \quad (5)$$

$$\begin{aligned} \text{Removal \% for AF} = & 93.65797 + 0.247032A - 0.427534B + 0.233538C \\ & + 0.103599AB - 0.033482AC \\ & + 0.000205BC + 0.438781A^2 \\ & - 0.000123B^2 - 0.000604C^2 \end{aligned} \quad (6)$$

Table 10 Calculated parameters of the confiscations of Cu(II) ions to SDA biochar employing the PFO and PSO models

Parameter			PFO model			PSO model			
SDA conc	Cu, (mg L ⁻¹)	q_e (exp.)	q_e (calc.)	$k_1 \times 10^3$	R^2	q_e (calc.)	$k_2 \times 10^3$	h	R^2
1.0 g L ⁻¹	50	49.44	4.569	68.1688	0.824	49.26	327.93	795,763.71	1.000
	75	69.72	26.853	63.3325	0.787	74.07	381.04	2,090,751.58	1.000
	100	73.33	15.733	28.0966	0.979	92.59	439.66	3,769,383.86	1.000
	125	90.83	74.046	61.7204	0.760	114.94	738.09	9,751,467.07	1.000
	150	96.67	256.33	58.9568	0.593	116.28	178.61	2,414,962.08	0.968
	175	101.39	49.705	4.606	0.694	123.46	173.40	2,642,841.08	0.962
	200	92.22	26.984	5.7575	0.435	89.29	95.70	762,926.86	0.977
1.5 g L ⁻¹	50	32.96	1.183	32.242	0.800	32.79	129.52	139,226.71	1.000
	75	49.63	5.043	18.424	0.886	49.50	269.31	660,013.97	1.000
	100	61.48	10.491	28.0966	0.912	66.23	302.47	1,326,551.79	1.000
	125	79.44	8.995	27.636	0.963	82.64	452.33	3,089,452.85	1.000
	150	82.04	23.394	6.909	0.788	93.46	172.96	1,510,683.59	0.994
	175	86.48	31.813	7.1393	0.867	98.04	131.49	1,263,810.43	0.988
	200	135.28	254.273	63.1022	0.596	84.75	58.63	421,052.14	0.956
2.0 g L ⁻¹	50	24.72	1.633	15.4301	0.957	24.75	40.04	24,534.83	1.000
	75	37.22	1.366	6.6787	0.137	37.31	160.03	222,813.54	1.000
	100	49.58	1.663	24.8724	0.812	49.75	353.60	875,221.00	1.000
	125	61.94	3.482	18.424	0.706	62.11	341.40	1,317,097.89	1.000
	150	71.25	9.436	9.4423	0.534	72.99	175.84	936,860.88	0.999
	175	74.72	16.908	6.909	0.612	80.65	119.33	776,098.34	0.995
	200	177.50	21.086	5.067	0.610	86.21	114.33	849,678.61	0.988
2.5 g L ⁻¹	50	19.63	1.364	62.181	0.812	19.80	23.34	9152.19	1.000
	75	29.78	2.213	66.3264	0.825	29.85	84.86	75,619.09	1.000
	100	39.78	3.739	70.4718	0.850	39.84	176.36	279,938.48	1.000
	125	49.67	7.779	51.5872	0.729	49.75	201.23	498,093.25	1.000
	150	58.67	35.686	55.7326	0.678	58.48	91.20	311,877.68	0.999
	175	65.78	76.12	57.8053	0.617	64.52	64.23	267,361.09	0.994
	200	175.83	14.0764	5.988	0.719	68.97	69.54	330,728.70	0.993
3.0 g L ⁻¹	50	16.36	3.919	62.181	0.812	16.50	13.55	3689.04	1.000
	75	24.82	1.199	23.9512	0.913	24.88	44.84	27,747.04	1.000
	100	33.241	1.521	21.4179	0.960	33.22	77.73	85,791.78	1.000
	125	41.481	1.483	57.8053	0.796	41.49	116.33	200,295.00	1.000
	150	49.167	3.816	55.7326	0.804	49.26	132.60	321,784.23	1.000
	175	56.574	8.849	58.7265	0.735	56.82	84.73	273,542.21	1.000
	200	191.389	80.984	70.0112	0.728	64.10	75.54	310,386.42	1.000

$$\begin{aligned} \text{Removal \% for CF} = & 73.76 + 10.88A - 19.37B + 18.29C - 0.7390AB \\ & - 1.424C + 1.98BC - 2.12A^2 - 0.0414B^2 - 10.74C^2 \end{aligned} \quad (7)$$

$$\begin{aligned} \text{Removal \% for AF} = & 42.40538 + 22.07450A - 0.264723B + 0.463204C \\ & - 0.009854AB - 0.016197AC + 0.000302BC - 2.11601A^2 \\ & - 7.35763 \times 10^{-6}B^2 - 0.001403C^2 \end{aligned} \quad (8)$$

$$\begin{aligned} \text{Removal \% for CF} = & 93.87 + 8.76A - 16.66B + 3.85C \\ & + 13.56AB - 0.4706AC + 5.86BC \\ & - 4.26A^2 - 14.544B^2 + 5.35C^2 \end{aligned} \quad (9)$$

$$\begin{aligned} \text{Removal \% for AF} = & 103.08349 + 3.71886AD - 0.019981B \\ & + 0.186031C + 0.180779AB \\ & - 0.005378AC + 0.000893BC - 4.26453A^2 \\ & - 0.002585B^2 + 0.000698C^2 \end{aligned} \quad (10)$$

The expressions in terms of AF could be utilized to make estimations about the response for specified levels of each factor. At this point, the levels should be quantified in the original units for each factor. This expression should not be employed to estimate the relative effect of each factor since the coefficients are scaled to manage

Table 11 Calculated parameters of the confiscations of Cu(II) ions to SD biochar employing the FD and IPD

SD dose	Cu(II) conc	Interparticle diffusions			Film diffusions		
		K_{dif}	C	R^2	K_{FD}	C	R^2
1.0 g L ⁻¹	50	1.3323	32.8370	0.522	0.0345	1.1927	0.889
	75	2.0167	38.0020	0.813	0.0128	1.0634	0.781
	100	2.0592	56.1030	0.939	0.0099	1.2914	0.913
	125	1.4593	56.6920	0.818	0.0166	1.6063	0.848
	150	2.4495	49.8100	0.963	0.0218	0.7868	0.842
	175	2.9443	64.6870	0.797	0.0135	1.2733	0.740
1.5 g L ⁻¹	50	0.3445	27.9850	0.906	0.0220	1.9622	0.963
	75	0.8649	34.5720	0.711	0.0249	1.4597	0.939
	100	1.1289	41.8020	0.939	0.0077	1.5979	0.889
	125	0.9974	46.8400	0.699	0.0162	1.8313	0.717
	150	0.7114	32.8570	0.777	0.0276	1.4548	0.980
	175	1.4350	52.1130	0.845	0.0151	1.5229	0.864
2.0 g L ⁻¹	50	0.2490	21.2440	0.902	0.0215	2.0273	0.970
	75	0.6503	27.8070	0.636	0.0139	1.7976	0.663
	100	0.5039	37.1410	0.916	0.0138	2.0549	0.929
	125	0.6589	44.3810	0.834	0.0214	1.8985	0.960
	150	0.7639	42.8380	0.947	0.0249	1.4974	0.972
	175	0.7702	49.2760	0.818	0.0166	1.9726	0.894
2.5 g L ⁻¹	50	0.1194	17.9290	0.956	0.0212	2.4235	0.956
	75	0.2706	25.6220	0.540	0.0314	2.3809	0.828
	100	0.3520	33.2710	0.753	0.0204	2.2723	0.886
	125	0.4720	38.9860	0.709	0.0129	2.3001	0.685
	150	0.6053	41.1830	0.771	0.0276	1.7713	0.982
	175	0.7856	46.3570	0.699	0.0249	1.9265	0.755
3.0 g L ⁻¹	50	0.0574	15.3830	0.998	0.0119	3.0366	0.997
	75	0.0961	22.8290	0.790	0.0209	3.0891	0.941
	100	0.1895	29.3740	0.692	0.0175	2.8662	2.866
	125	0.1277	37.2290	0.971	0.0137	3.2979	3.298
	150	0.5329	37.3230	0.837	0.0227	1.5557	1.856
	175	0.6649	41.4470	0.718	0.0255	1.8331	1.833

the units of each factor and the intercept is not at the midpoint of the design space.

A correlation between projected and actual adsorption (%) of Cu(II) ions on SD, SSD, and SDA biochars is illustrated in Fig. 15. It is obvious from the figure (Fig. 15) that there are good correlations between the experimental values and the projected model, and this is authenticated by the high value of the correlation coefficient ($R^2 = 0.9931$ for SD biochar; 0.9915 for SSD biochar, and 0.9545 for SDA biochar). The ANOVA for SD, SSD, and SDA biochars are given in Tables 15, 16 and 17, respectively, and is employed in predicting the cubic, individual, and interaction impact of the independent variables on the adsorption of Cu(II) ions on SD biochar. The results propose that the quadratic model (P -value < 0.05) has significant contributions. The determination coefficient defined the standard of the polynomial model as a basis of the degree of deviations using the average (mean) explicated

by the model, and the values of adj- R^2 and R^2 show a good correlation between the projected and exponential data [88–91]. The projected R^2 of 0.9768 (SD), 0.9388 (SSD), and 0.7086 (SDA) is in realistic agreement with the adjusted R^2 of 0.9870 (SD), 0.9839 (SSD), and 0.9136 (SDA). Adeq precisions measure the signal to noise (S/N) ratio. A ratio greater than 4 is desirable. The S/N value 44.7319 (SD), 39.2612 (SSD), and 17.5015 (SDA) indicate an adequate signal, which shows significant RSM model indications that can be employed for the navigations of the design [90, 92].

3.9 The simultaneous impacts of the interactive adsorption variables

The 3-D surface plots present the impacts and interactions of independent variables, viz., adsorbent dose (A: g L⁻¹), initial Cu(II) ion conc (B: mg L⁻¹), and contact

Table 12 Calculated parameters of the confiscations of Cu(II) ions to SSD biochar employing the FD and IPD

SSD dose	Cu(II) conc	IPD model			FD model		
		K_{dif}	C	R^2	K_{FD}	C	R^2
1.0 g L ⁻¹	50	0.0279	1.3557	0.937	0.0260	0.4637	0.932
	75	0.0383	1.3919	0.947	0.0619	−1.0864	0.774
	100	0.0392	1.4493	0.896	0.0172	0.4373	0.962
	125	0.0419	1.4562	0.938	0.0102	0.4004	0.930
	150	0.0446	1.4775	0.935	0.0595	−1.3744	0.640
	175	0.0449	1.4629	0.976	0.0089	0.3329	0.973
	200	0.0445	1.4583	0.883	0.0094	0.4226	0.924
1.5 g L ⁻¹	50	0.0169	1.3216	0.819	0.0511	0.1143	0.798
	75	0.0183	1.4758	0.886	0.0569	−0.2322	0.788
	100	0.0266	1.4602	0.880	0.0554	−0.5928	0.743
	125	0.0303	1.4062	0.950	0.0520	−0.9268	0.660
	150	0.0258	1.5056	0.964	0.0141	0.5858	0.821
	175	0.0312	1.4980	0.893	0.0102	0.6063	0.904
	200	0.0342	1.4626	0.843	0.0098	0.5760	0.866
2.0 g L ⁻¹	50	0.0158	1.2047	0.848	0.0220	1.1162	0.969
	75	0.0181	1.3503	0.828	0.0214	1.0226	0.963
	100	0.0240	1.3786	0.884	0.0203	0.7392	0.939
	125	0.0252	1.4302	0.922	0.0507	−0.5196	0.727
	150	0.0300	1.4056	0.872	0.0534	−0.6046	0.755
	175	0.0303	1.4454	0.908	0.0569	−0.8816	0.683
	200	0.0298	1.4522	0.837	0.0521	−0.7920	0.674
2.5 g L ⁻¹	50	0.0075	1.2087	0.869	0.0463	1.0676	0.896
	75	0.0124	1.3251	0.873	0.0294	1.2135	0.975
	100	0.0172	1.3672	0.857	0.0233	0.9646	0.890
	125	0.0211	1.3987	0.922	0.0250	0.6530	0.841
	150	0.0209	1.4100	0.940	0.0515	0.3681	0.756
	175	0.0242	1.4304	0.905	0.0205	0.6498	0.878
	200	0.0283	1.4040	0.836	0.0124	0.6568	0.826
3.0 g L ⁻¹	50	0.0051	1.1567	0.791	0.0476	1.4182	0.860
	75	0.0081	1.2948	0.823	0.0503	0.8735	0.856
	100	0.0110	1.3798	0.838	0.0322	1.2271	0.871
	125	0.0163	1.3940	0.852	0.0519	0.1819	0.877
	150	0.0196	1.3834	0.858	0.0552	−0.3270	0.749
	175	0.0198	1.4322	0.887	0.0191	0.8836	0.972
	200	0.0278	1.3765	0.801	0.0145	0.7270	0.886

time (C: min), on the percentage of removal of Cu(II) ions using SD, SSD, and SDA biochars (Fig. 16, 17 and 18) as the responses. The interactions of initial ion conc and adsorbent dosage as illustrated in Fig. 16a–c specify the significant impact of both factors for Cu(II) ion removal utilizing the SD, SSD, and SDA biochars. The percentage of removal rise with corresponding rising adsorbent biochar dosage. This was a result of the existence of

additional active sites and a large adsorbent surface area that is eagerly accessible for the adsorption [89, 93]. The percentage of removal was reduced by the rising of the initial Cu(II) ion conc (Fig. 17a–c). This finding is possibly due to the inadequate active spots on the adsorbent surface at high biochar conc [94]. The percentage of removal was increased by rising the contact time (Fig. 18a–c). These results certified that the initial adsorption rate was very

Table 13 Calculated parameters of the confiscations of Cu(II) ions to SDA biochar employing the FD and IPD

SDA dose	Cu(II) conc	IPD model			FD model		
		K_{dif}	C	R^2	K_{FD}	C	R^2
1.0 g L ⁻¹	50	0.0017	1.6728	0.652	0.0241	3.3833	0.780
	75	0.0046	1.8164	0.708	0.0236	2.3539	0.832
	100	0.0075	1.8803	0.792	0.0284	1.7595	0.958
	125	0.0082	1.9639	0.797	0.0260	1.7031	0.929
	150	0.0119	1.8881	0.754	0.0033	1.1867	0.513
	175	0.0181	1.8385	0.825	0.0060	0.9264	0.686
	200	0.0143	1.7575	0.645	0.0048	1.2540	0.202
1.5 g L ⁻¹	50	0.0009	1.5047	0.7975	0.0166	3.912	0.788
	75	0.0016	1.6758	0.841	0.0185	3.350	0.886
	100	0.0045	1.7682	0.673	0.0259	2.4116	0.817
	125	0.0055	1.8530	0.739	0.0283	2.1026	0.928
	150	0.0094	1.8422	0.878	0.0085	1.4958	0.768
	175	0.0124	1.8172	0.898	0.0058	1.2719	0.719
	200	0.0158	1.7007	0.800	0.0055	0.9713	0.746
2.0 g L ⁻¹	50	0.0010	1.3809	0.954	0.0154	3.6981	0.957
	75	0.0013	1.5562	0.790	0.0239	3.5181	0.910
	100	0.0020	1.675	0.562	0.0322	3.2189	0.843
	125	0.0032	1.7563	0.675	0.0242	2.7421	0.713
	150	0.0070	1.7762	0.632	0.0149	1.9203	0.669
	175	0.0099	1.7773	0.670	0.0087	1.5375	0.571
	200	0.0104	1.7920	0.804	0.0071	1.3906	0.638
2.5 g L ⁻¹	50	0.0010	1.2842	0.928	0.0185	3.7053	0.897
	75	0.0012	1.4607	0.852	0.0227	3.5972	0.937
	100	0.0019	1.5788	0.655	0.0324	3.2028	0.861
	125	0.0028	1.6636	0.580	0.0218	2.9309	0.664
	150	0.0068	1.6833	0.778	0.0155	1.9167	0.758
	175	0.0085	1.6936	0.767	0.0088	1.5770	0.710
	200	0.0090	1.7142	0.857	0.0080	1.5115	0.755
3.0 g L ⁻¹	50	0.0010	1.2050	0.928	0.0185	3.7053	0.897
	75	0.0013	1.3796	0.763	0.0239	3.4772	0.913
	100	0.0016	1.5020	0.859	0.0206	3.2691	0.916
	125	0.0021	1.5921	0.894	0.0205	2.9930	0.954
	150	0.0044	1.6435	0.653	0.0294	2.3743	0.882
	175	0.0073	1.6666	0.825	0.0194	1.8333	0.916
	200	0.0091	1.6918	0.867	0.0110	1.6837	0.766

fast owing to the accessibility of the huge surface area and the existence of unexploited spots on the biochar surface [95, 96]. The retardations of Cu(II) ion removal were a result of the difficulty of attaining the residual vacant sites.

To optimize and validate the predicted mathematical model, complementary statistical design calculations were performed under the same experimental conditions; Fig. 19 shows that the higher desirability value is equal to 1 obtained from the results of the mathematical model. Using these conditions, the maximum removal

(%) (99.343%) for the SD biochar as adsorbent was obtained corresponding to the contact time 139.8 min, SD biochar dose 2.853 g L⁻¹, and Cu(II) ion conc of 55.11 mg L⁻¹ (Fig. 19a). Figure 19b shows that the maximum removal (%) (100%) obtained corresponds to the contact time 180 min, SSD biochar dose 3.0 g L⁻¹, and Cu(II) ion conc of 75 mg L⁻¹. Figure 19c shows that the maximum removal (%) (100%) obtained corresponds to the contact time 30 min, SDA biochar dose 2 g L⁻¹, and Cu(II) ion conc of 50 mg L⁻¹.

Table 14 Experimental design for adsorption of Cu(II) ions on SD biochar, SSD biochar and SDA biochar

Run	Independent factors			Response %	
	A	B	C	Exp	Predicted
SD biochar					
1	1	100	15	63.06	63.89
2	3	175	180	84.44	84.99
3	3	50	180	97.78	98.42
4	3	50	15	93.89	94.22
5	1	175	120	54.13	53.5
6	3	50	15	93.89	94.22
7	3	125	90	92.22	91.23
8	2.5	175	15	66.19	66.41
9	2	50	90	95.56	95.6
10	1	50	180	95.56	96.11
11	2	125	180	83.78	81.46
12	1.5	125	90	68.44	72.99
13	1	175	15	38.25	37.3
14	3	125	90	92.22	91.23
15	2.5	175	15	66.19	66.41
16	1	50	180	95.56	96.11
17	3	175	180	84.44	84.99
18	2	50	180	97.22	96.83
19	2	100	15	76.39	75.32
20	1	50	90	93.89	91.87
SSD biochar					
1	3	175	180	80.16	76.56
2	1	200	180	53.06	53.05
3	1	175	90	44.29	47.72
4	3	50	60	96.11	95.59
5	3	150	90	74.26	75.31
6	3	50	60	96.11	95.59
7	3	200	5	32.64	32.77
8	2	200	90	50.28	53.76
9	1	200	180	53.06	53.05
10	1	100	120	74.72	71.9
11	3	200	5	32.64	32.77
12	1	125	15	32.89	34.88
13	1	50	5	50.00	50.89
14	1	50	5	50.00	50.89
15	2	75	90	91.11	86.17
16	2	50	180	97.78	98.67
17	2	125	5	44.44	44.73
18	1	200	5	14.03	9.66
19	3	75	180	97.41	100.73
20	2	125	5	44.44	44.73
SDA biochar					
1	1	50	60	97.78	97.82
2	2	50	30	97.22	100.14
3	1	50	60	97.78	97.82
4	3	50	5	96.67	94.74
5	3	100	120	99.17	98.76

Table 14 (continued)

Run	Independent factors			Response %	
	A	B	C	Exp	Predicted
6	1.5	200	120	49.72	54.1
7	3	125	30	97.11	98.68
8	3	50	5	96.67	94.74
9	1	125	180	91.33	90.51
10	1	200	5	26.11	31.25
11	2.5	175	90	84.44	83.92
12	1	125	180	91.33	90.51
13	2	125	5	89.33	95.36
14	1	125	30	85.78	80.48
15	2	50	180	98.89	99.32
16	2	200	15	70.97	58.26
17	3	200	180	95.69	95.31
18	3	200	180	95.69	95.31
19	2	50	180	98.89	99.32
20	3	200	5	72.64	76.83

4 Conclusions

Low-cost biochar derived from sawdust biomass is burned with sulfuric acid to give SD biochar, then activated with sonications to give SSD biochar, and chemically modified by NH_4OH to give SDA biochar. The characterizations of SD, SSD, and SDA biochars using FTIR spectroscopy showed obvious differences between them in the disappearance of carboxylic FGs and the presence of amino groups in chemically modified biochar. Also, EDX analysis showed the absence of nitrogen in SD and SSD biochars and the presence of a new peak for nitrogen in SDA biochar after modifications. Cu(II) ions are removed by these biochars from their water solutions. The LNR isotherm model was best fitted to the experimental data of SD, SSD, and SDA. The maximum adsorption capacities (Q_m) of SD, SSD, and SDA were 91.74, 112.36, and 133.33 mg g^{-1} , respectively. The degree of fitting using the non-linear isotherm models was in the sequence of LNR (ideal fit) > FRH > Temkin (SD and SSD) and FRH (ideal fit) > LNR > Temkin (SDA). LNR and FRH ideally described the biosorption of Cu(II) ions to SD and SSD and SDA owing to the low values of χ^2 and R^2 obtained using the non-linear isotherm models. The adsorption rate was well-ordered by the PSO rate model. Finally, the chemical modifications of sawdust biochar by ammonia enhance the adsorption

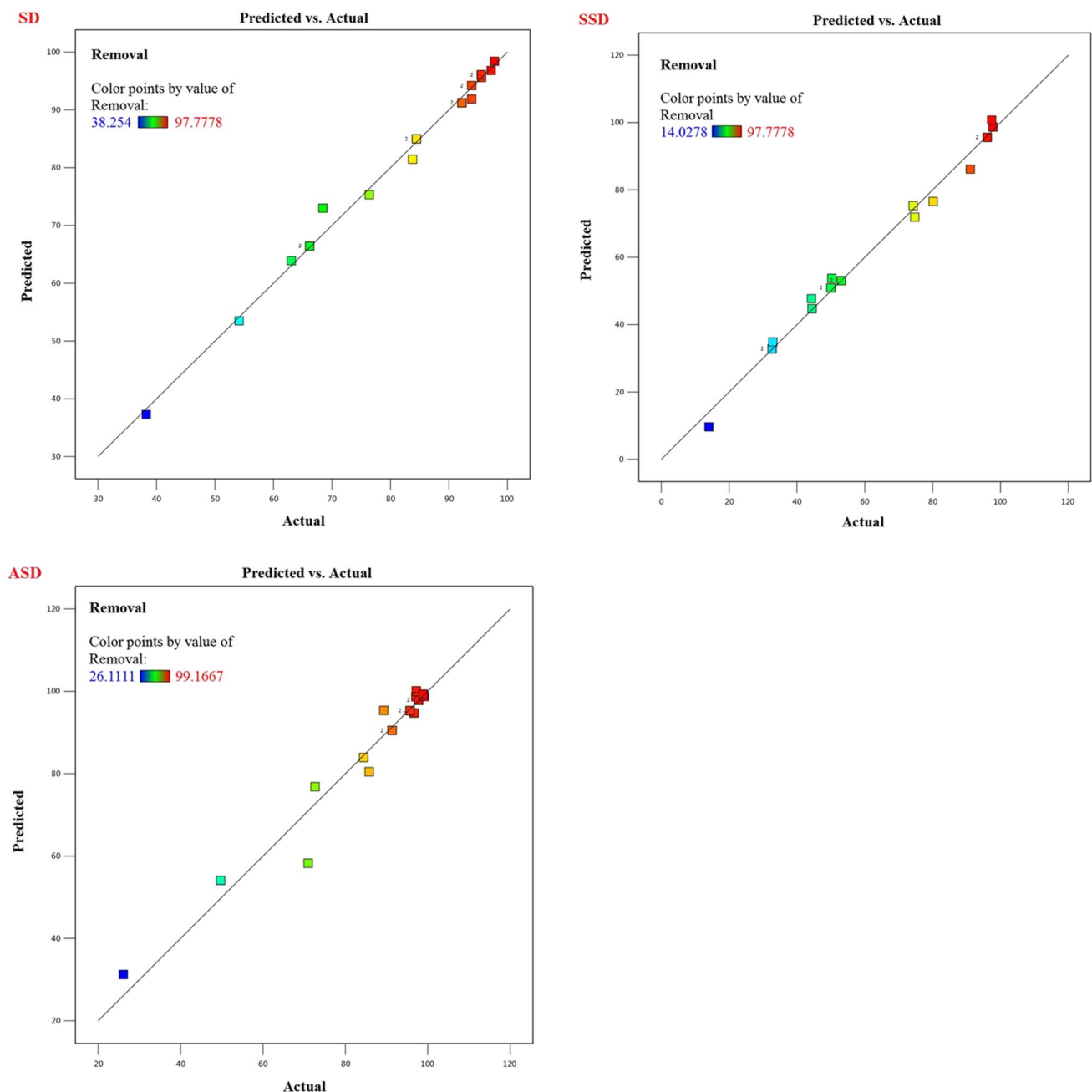


Fig. 15 Plots (graphs) between the projected and experimental data for Cu(II) ion adsorption

efficiency more than physical activations by sonications. The findings of this study have further suggested that biosorbents made from waste agro-based by-products, which are low-cost agricultural waste materials, can be effective in removing other HMs from wastewater.

Hence, it is suggested that more investigations into the use of more readily available agro-based by-products as low-cost (cheap) adsorbents for environmental and agricultural sustainability should be reinvestigated.

Table 15 ANOVA and model fit summary for D-optimal design of Cu(II) ion removal using SD biochar

Source	Value	Sum of squares	df	Mean square	F-value	P-value	Remarks	Source	Std	R ²	Adjusted R ²	Predicted R ²	PRESS	Remarks
Model	-	5404.95	9	600.55	160.81	<0.0001	Significant	-	-	-	-	-	-	-
A—dose	-	1182.17	1	1182.17	316.55	<0.0001	-	-	-	-	-	-	-	-
B—conc	-	2195.21	1	2195.21	587.82	<0.0001	-	-	-	-	-	-	-	-
C—time	-	363.21	1	363.21	97.26	<0.0001	-	-	-	-	-	-	-	-
AB	-	355.79	1	355.79	95.27	<0.0001	-	-	-	-	-	-	-	-
AC	-	54.51	1	54.51	14.6	0.0034	-	-	-	-	-	-	-	-
BC	-	9.17	1	9.17	2.45	0.1482	-	-	-	-	-	-	-	-
A ²	-	0.61	1	0.61	0.16	0.6936	-	-	-	-	-	-	-	-
B ²	-	0.69	1	0.69	0.18	0.6767	-	-	-	-	-	-	-	-
C ²	-	58.83	1	58.83	15.75	0.0026	-	-	-	-	-	-	-	-
Residual	-	37.34	10	3.73	-	-	-	-	-	-	-	-	-	-
Lack of fit	-	37.34	5	7.47	-	-	-	-	-	-	-	-	-	-
Pure error	-	0	5	0	-	-	-	-	-	-	-	-	-	-
Cor total	-	5442.3	19	-	-	-	-	-	-	-	-	-	-	-
SD	1.93	-	-	-	-	-	-	-	-	-	-	-	-	-
Mean	81.65	-	-	-	-	-	-	-	-	-	-	-	-	-
C.V.%	2.37	-	-	-	-	-	-	-	-	-	-	-	-	-
R ²	0.9931	-	-	-	-	-	-	-	-	-	-	-	-	-
Adjusted R ²	0.9870	-	-	-	-	-	-	-	-	-	-	-	-	-
Predicted R ²	0.9768	-	-	-	-	-	-	-	-	-	-	-	-	-
Adeq Precisions	44.7319	-	-	-	-	-	-	-	-	-	-	-	-	-
Linear	-	-	-	-	-	-	-	-	6.05	0.8923	0.8721	0.8211	973.42	-
2FI	-	-	-	-	-	-	-	-	2.87	0.9804	0.9713	0.9544	248.17	-
Quadratic	-	-	-	-	-	-	-	-	1.93	0.9931	0.9870	0.9768	126.02	Suggested
Cubic	-	-	-	-	-	-	-	-	0.0000	1.0000	1.0000	-	*	Aliased

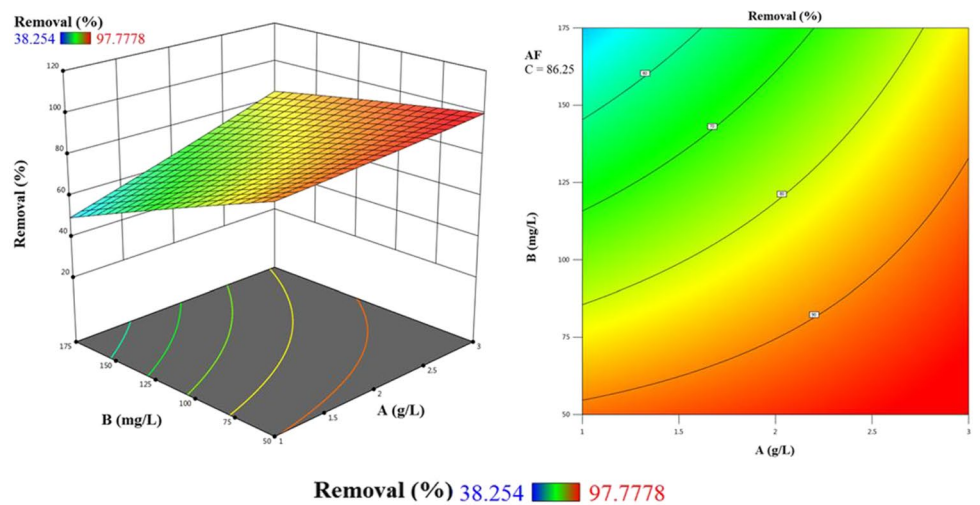
Table 16 ANOVA and model fit summary for D-optimal design for adsorption of Cu(II) ions by SSD biochar

Source	Value	Sum of squares	df	Mean square	F-value	P-value	Remarks	Source	SD	R ²	Adjusted R ²	Predicted R ²	PRESS	Remarks
Model	-	12584.38	9	1398.26	129.92	<0.0001	Significant	-	-	-	-	-	-	-
A—dose	-	1327.79	1	1327.79	123.37	<0.0001	-	-	-	-	-	-	-	-
B—conc	-	3541.07	1	3541.07	329.01	<0.0001	-	-	-	-	-	-	-	-
C—time	-	3392.55	1	3392.55	315.21	<0.0001	-	-	-	-	-	-	-	-
AB	-	4.40	1	4.40	0.4092	0.5367	-	-	-	-	-	-	-	-
AC	-	14.02	1	14.02	1.30	0.2804	-	-	-	-	-	-	-	-
BC	-	26.75	1	26.75	2.49	0.1460	-	-	-	-	-	-	-	-
A ²	-	14.45	1	14.45	1.34	0.2734	-	-	-	-	-	-	-	-
B ²	-	0.0048	1	0.0048	0.0004	0.9836	-	-	-	-	-	-	-	-
C ²	-	379.43	1	379.43	35.25	0.0001	-	-	-	-	-	-	-	-
Residual	-	107.63	10	10.76	-	-	-	-	-	-	-	-	-	-
Lack of fit	-	107.63	5	21.53	1.088E+09	<0.0001	Significant	-	-	-	-	-	-	-
Pure error	-	9.889E-08	5	1.978E-08	-	-	-	-	-	-	-	-	-	-
Cor total	-	12692.00	19	-	-	-	-	-	-	-	-	-	-	-
SD	3.28	-	-	-	-	-	-	-	-	-	-	-	-	-
Mean	60.47	-	-	-	-	-	-	-	-	-	-	-	-	-
C.V.%	5.43	-	-	-	-	-	-	-	-	-	-	-	-	-
R ²	0.9915	-	-	-	-	-	-	-	-	-	-	-	-	-
Adjusted R ²	0.9839	-	-	-	-	-	-	-	-	-	-	-	-	-
Predicted R ²	0.9388	-	-	-	-	-	-	-	-	-	-	-	-	-
Adeq precisions	39.2612	-	-	-	-	-	-	-	-	-	-	-	-	-
Linear	-	-	-	-	-	-	-	-	6.59	0.9453	0.9350	0.9154	1073.50	-
2FI	-	-	-	-	-	-	-	-	6.44	0.9575	0.9379	0.9020	1243.46	-
Quadratic	-	-	-	-	-	-	-	-	3.28	0.9915	0.9839	0.9388	777.17	Suggested
Cubic	-	-	-	-	-	-	-	-	0.0001	1.0000	1.0000	-	*	Aliased

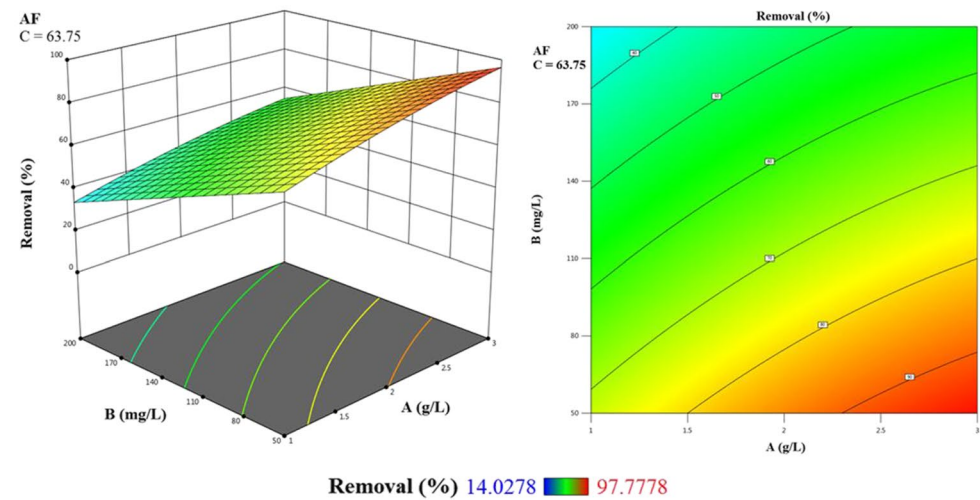
Table 17 ANOVA and model fit summary for D-optimal design for removal of Cu(II) ions using SDA biochar

Source	Value	Sum of squares	df	Mean square	F-value	P-value	Remarks	Source	SD	R ²	Adjusted R ²	Predicted R ²	PRESS	Remarks
Model	-	6506.90	9	722.99	23.33	<0.0001	Significant	-	-	-	-	-	-	-
A—dose	-	819.97	1	819.97	26.46	0.0004	-	-	-	-	-	-	-	-
B—conc	-	2994.30	1	2994.30	96.63	<0.0001	-	-	-	-	-	-	-	-
C—time	-	167.89	1	167.89	5.42	0.0422	-	-	-	-	-	-	-	-
AB	-	1182.74	1	1182.74	38.17	0.0001	-	-	-	-	-	-	-	-
AC	-	1.48	1	1.48	0.0479	0.8311	-	-	-	-	-	-	-	-
BC	-	235.61	1	235.61	7.60	0.0202	-	-	-	-	-	-	-	-
A ²	-	57.09	1	57.09	1.84	0.2045	-	-	-	-	-	-	-	-
B ²	-	694.65	1	694.65	22.42	0.0008	-	-	-	-	-	-	-	-
C ²	-	67.77	1	67.77	2.19	0.1700	-	-	-	-	-	-	-	-
Residual	-	309.89	10	30.99	-	-	-	-	-	-	-	-	-	-
Lack of fit	-	309.89	5	61.98	-	-	-	-	-	-	-	-	-	-
Pure error	-	0.0000	5	0.0000	-	-	-	-	-	-	-	-	-	-
Cor total	-	6816.79	19	-	-	-	-	-	-	-	-	-	-	-
SD	5.57	-	-	-	-	-	-	-	-	-	-	-	-	-
Mean	86.66	-	-	-	-	-	-	-	-	-	-	-	-	-
C.V.%	6.42	-	-	-	-	-	-	-	-	-	-	-	-	-
R ²	0.9545	-	-	-	-	-	-	-	-	-	-	-	-	-
Adjusted R ²	0.9136	-	-	-	-	-	-	-	-	-	-	-	-	-
Predicted R ²	0.7086	-	-	-	-	-	-	-	-	-	-	-	-	-
Adeq precisions	17.5015	-	-	-	-	-	-	-	-	-	-	-	-	-
Linear	-	-	-	-	-	-	-	-	11.81	0.6727	0.6113	0.4340	3858.36	-
2FI	-	-	-	-	-	-	-	-	8.84	0.8508	0.7820	0.5123	3324.60	-
Quadratic	-	-	-	-	-	-	-	-	5.57	0.9545	0.9136	0.7086	1986.61	Suggested
Cubic	-	-	-	-	-	-	-	-	0.0000	1.0000	1.0000	-	*	Aliased

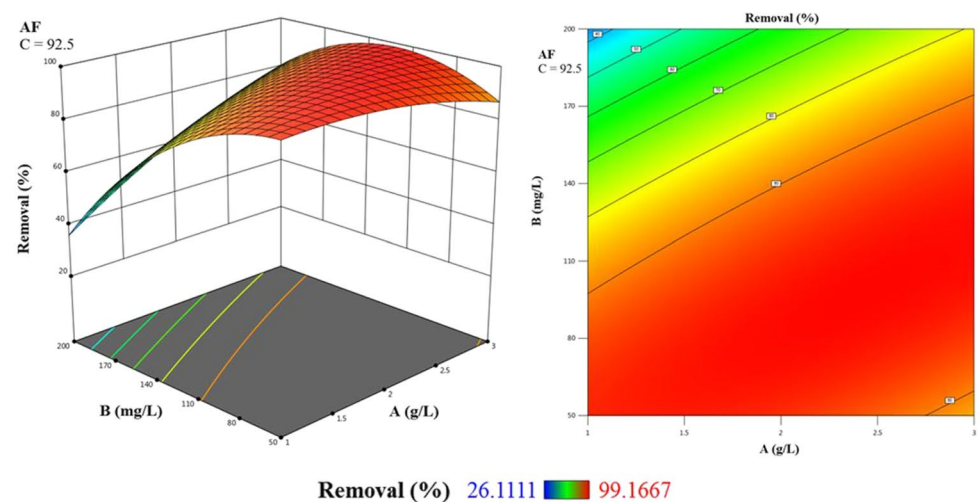
Fig. 16 Combined effect of process variables of Cu(II) ion initial conc (mg L^{-1}) and adsorbent doses (g L^{-1}) of **a** SD biochar, **b** SSD biochar, and **c** SDA biochar with the interaction effect of dual factors



(a) SD biochar

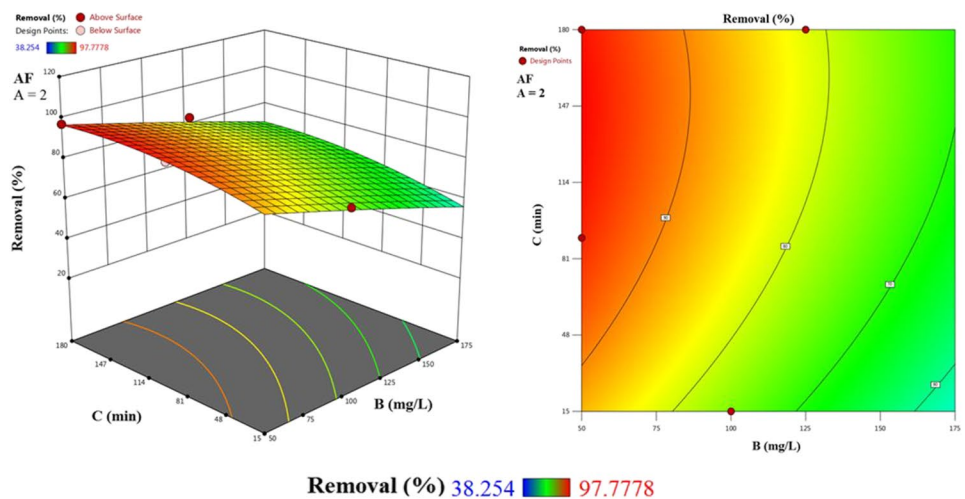


(b) SSD biochar

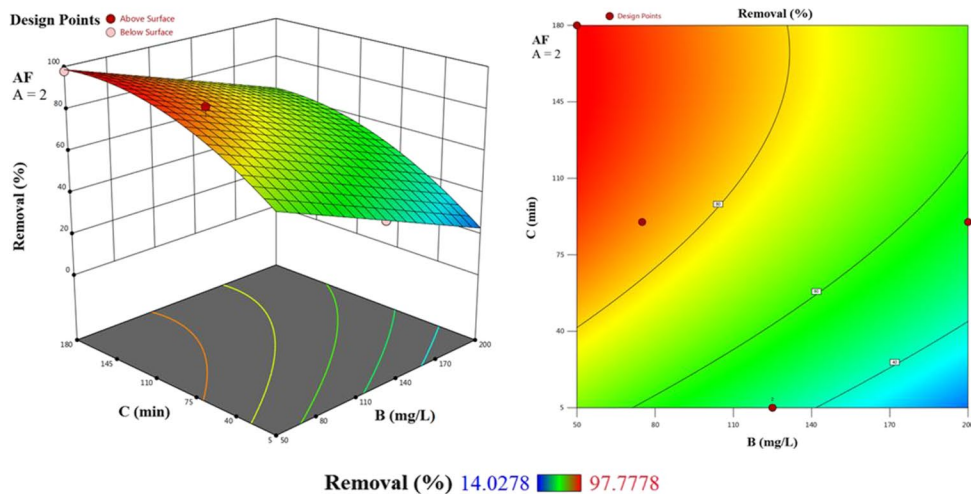


(c) SDA biochar

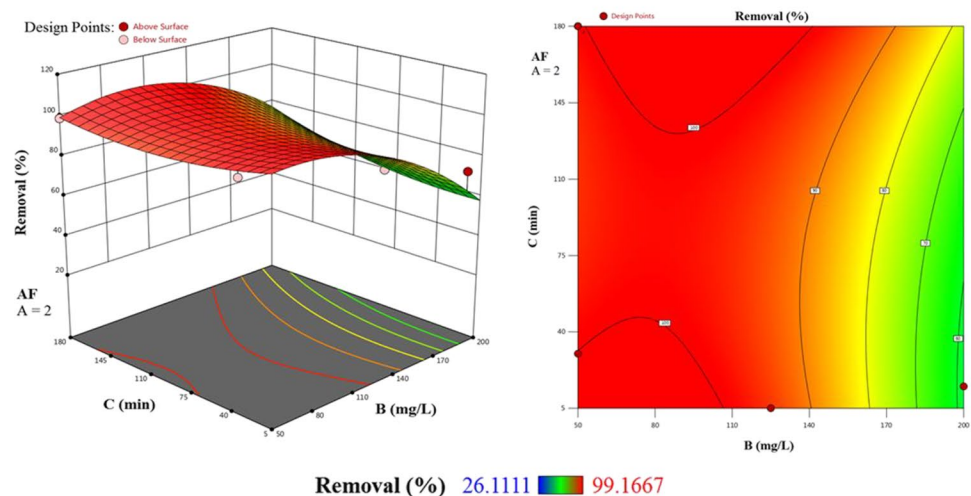
Fig. 17 Combined effect of process variables of Cu(II) ion initial conc (mg L^{-1}) and contact time (min) **a** SD biochar, **b** SSD biochar, and **c** SDA biochar with the interactions effect of dual factors



(a) SD biochar

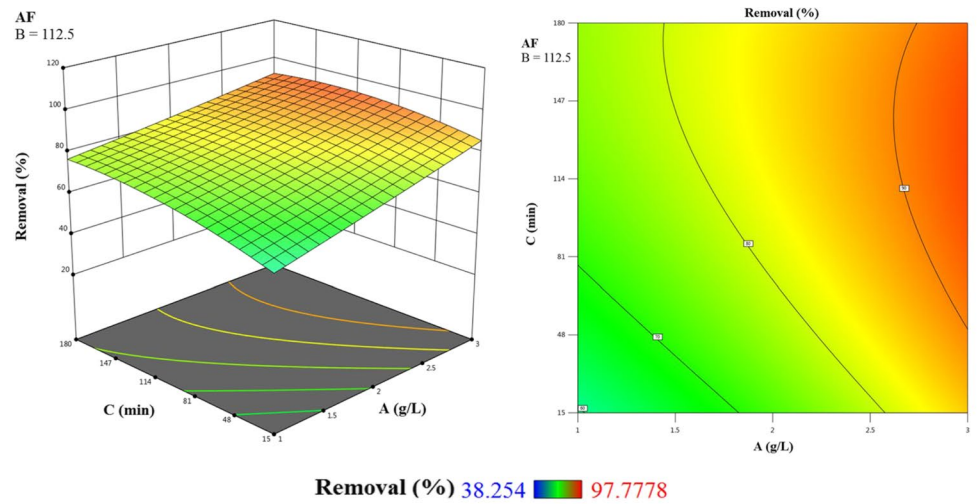


(b) SSD biochar

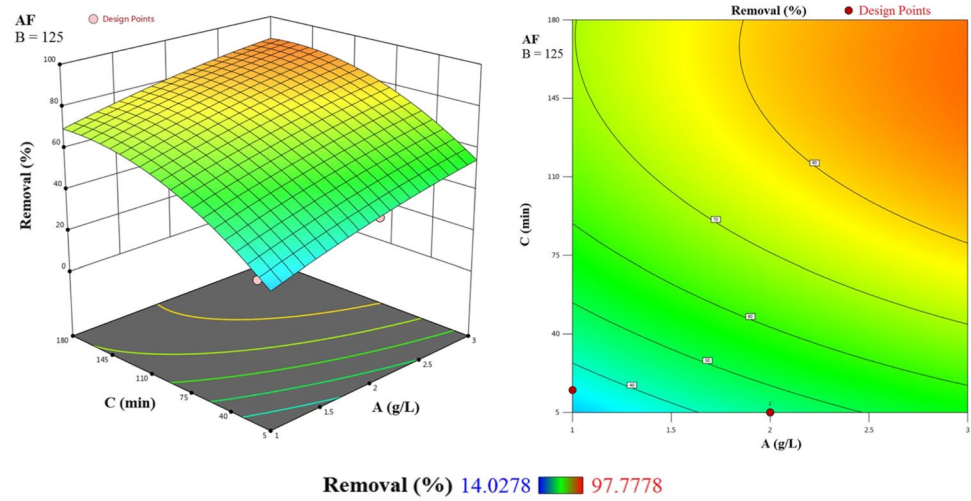


(c) SDA biochar

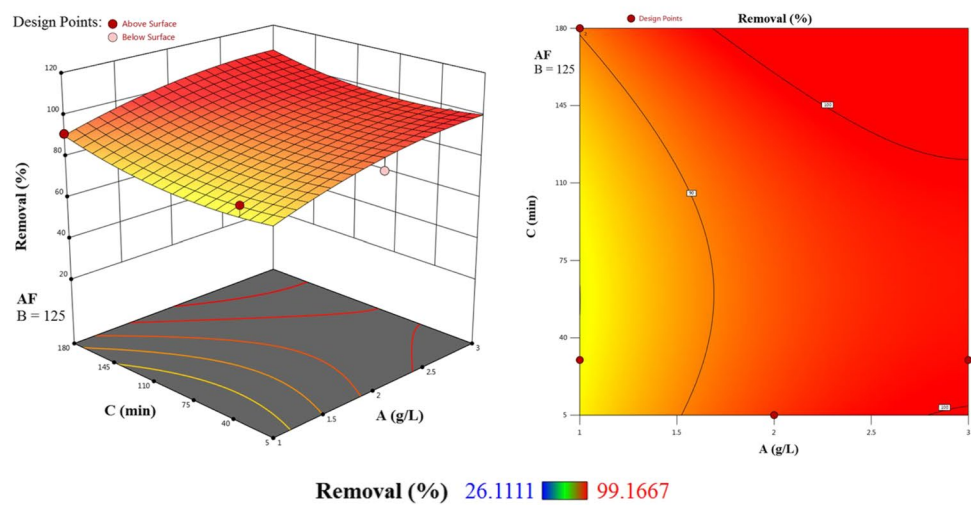
Fig. 18 Combined effect of process variables adsorbent doses (g L^{-1}) and contact time (min) **a** SD biochar, **b** SSD biochar, and **c** SDA biochar with the interactions effect of dual factors



(a) SD biochar

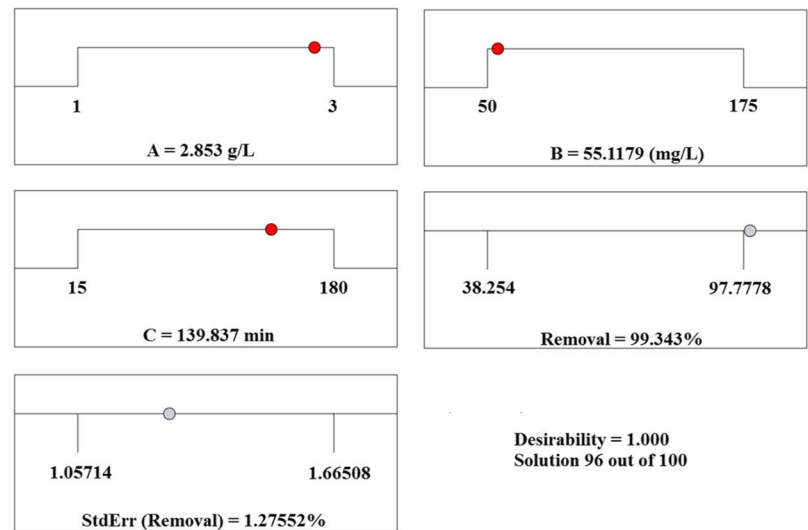


(b) SSD biochar

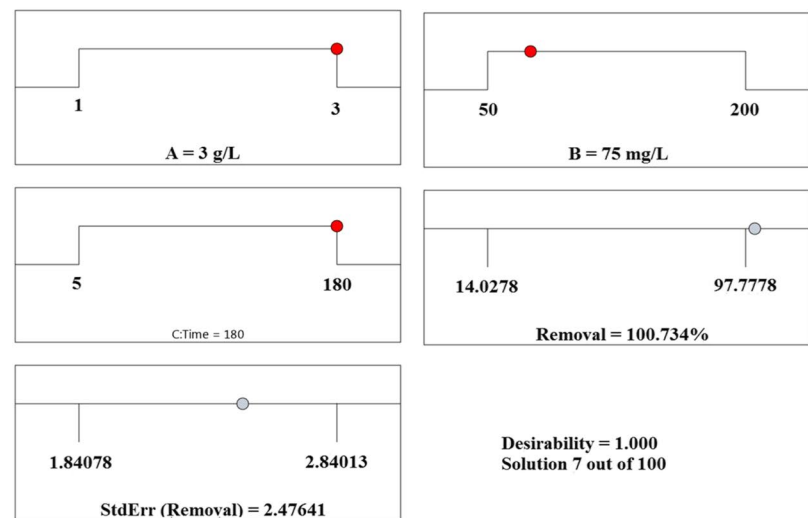


(c) SDA biochar

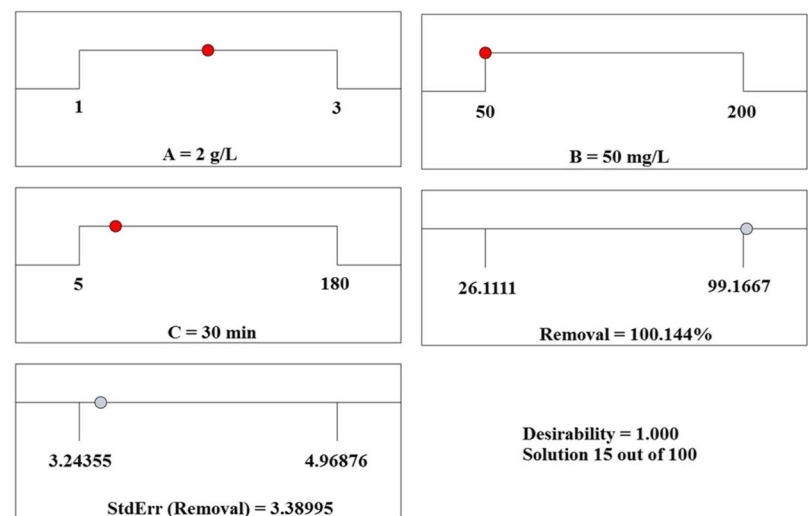
Fig. 19 Optimum conditions are predicted by the RSM method for **a** SD biochar, **b** SSD biochar, and **c** SDA biochar



(a) SD biochar



(b) SSD biochar



(c) SDA biochar

Author contribution Dr. A. Eleryan, Mr. T.M. Eldeeb, and Engr. M.A. El-Nemr carried out the experiment, calculation, and theoretical models. M.A. Hassaan carried out the calculations and characterization, Dr. S. Ragab read the manuscript and supervised the experimental work, and Dr. U.O. Aigbe, Dr. K.E. Ukhurebor, Dr. R.B. Onyancha, Dr. O.A. Osibote, Prof. H.S. Kusuma, and Prof. H. Darmokoesoemo carried out the calculations, theoretical models, wrote the original manuscript, and revised the manuscript after review. Prof. A. El Nemr supervised the experimental work, completed the manuscript, and provided financial support for the experiment work.

Funding Open access funding provided by The Science, Technology & Innovation Funding Authority (STDF) in cooperation with The Egyptian Knowledge Bank (EKB). This work was partially funded by the Science and Technology Development Fund (STDF) of Egypt (Projects Nos. CB-4874 and CB-22816).

Data availability Data sharing does not apply to this article.

Declarations

Consent to participate Not applicable

Conflict of interest The authors declare no competing interests.

Open Access This article is licensed under a Creative Commons Attribution 4.0 International License, which permits use, sharing, adaptation, distribution and reproduction in any medium or format, as long as you give appropriate credit to the original author(s) and the source, provide a link to the Creative Commons licence, and indicate if changes were made. The images or other third party material in this article are included in the article's Creative Commons licence, unless indicated otherwise in a credit line to the material. If material is not included in the article's Creative Commons licence and your intended use is not permitted by statutory regulation or exceeds the permitted use, you will need to obtain permission directly from the copyright holder. To view a copy of this licence, visit <http://creativecommons.org/licenses/by/4.0/>.

References

1. El Nemr (2005) Petroleum contaminations in warm and cold marine environment. Nova Science Publishers, Inc. Hauppauge New York. [ISBN 1–59454–615–0] 150pp
2. Sudarni DHA, Aigbe UO, Ukhurebor KE, Onyancha RB, Kusuma HS, Darmokoesoemo H, Osibote OA, Balogun VA, Widyandin-grum BA (2021) Malachite green removal by activated potassium hydroxide clove leaves agro-waste biosorbent: characterizations, kinetics, isotherms and thermodynamics studies. *Adsorp Sci Tech* 1145312:1–15
3. Aigbe UO, Onyancha RB, Ukhurebor KE, Obodo KO (2020) Removal of fluoride ions using polypyrrole magnetic nanocomposite influenced by rotating magnetic field. *RSC Adv* 10(1):595–609
4. Ukhurebor KE, Aigbe UO, Onyancha RB, Nwankwo W, Osibote OA, Paumo HK, Ama OM, Adetunji CO, Siloko IU (2021) Effect of hexavalent chromium on the environment and removal techniques: a review. *J Environ Manag* 280:11180
5. Ismael MN, El Nemr A, El Sayed H, Hamid HA (2020) Removal of hexavalent chromium by cross-linking chitosan and *N*, *N*'-methylene bis-acrylamide. *Environ Processes* 7:911–930
6. Hosain AN, El Nemr A, El Sikaily A, Mahmoud ME, Amira MF (2020) Surface modifications of nanochitosan coated magnetic nanoparticles and their applications in Pb(II), Cu(II) and Cd(II) removal. *J Environ Chem Eng* 8(5):104316
7. El Nemr A, El-Assal AA, El Sikaily A, Mahmoud ME, Amira MF, Ragab S (2021) New magnetic cellulose nanobiocomposites for Cu(II), Cd(II) and Pb(II) ions removal: kinetics, thermodynamics and analytical evaluations. *Nanotech Environ Eng* 6(3):1–20
8. El-Nemr MA, Abdelmonem NM, Ismail IM, Ragab S, El Nemr A (2020) Ozone and ammonium hydroxide modifications of biochar prepared from *pisum sativum* peels improves the adsorptions of copper (II) from an aqueous medium. *Environ Process* 7(3):973–1007
9. Eldeeb TM, El Nemr A, Khedr MH, El-Dek SI (2021) Efficient removal of Cu(II) from water solutions using magnetic chitosan nanocomposite. *Nanotech Environ Eng* 6(2):1–15
10. Dehghani MH, Omrani GA, Karri RR (2021) Solid waste—sources, toxicity, and their consequences to human health, Editor(s): Karri RR, Ravindran G, Dehghani, MH. *Soft computing techniques in solid waste and wastewater management*, Elsevier, 11: 205–213. <https://doi.org/10.1016/B978-0-12-824463-0.00013-6>
11. Karri RR, Ravindran G, Dehghani MH (2021) Wastewater—sources, toxicity, and their consequences to human health, Editor(s): Karri RR, Ravindran G, Dehghani, MH. *Soft computing techniques in solid waste and wastewater management*, Elsevier, 1: 3–33. <https://doi.org/10.1016/B978-0-12-824463-0.00001-X>
12. Aigbe UO, Ukhurebor KE, Onyancha RB, Osibote OA, Darmokoesoemo H, Kusuma HS (2021) Fly ash-based adsorbent for adsorptions of heavy metals and dyes from aqueous solutions: a review. *J Mater Res Technol* 14:2751–2774
13. Ibrahim E, Moustafab H, El-molla SA, Halim SD, Ibrahim SS (2021) Integrated experimental and theoretical insights for malachite green dye adsorptions from wastewater using low-cost adsorbent. *Water Sci Technol* 1–26
14. El Nemr A (2011) Impact, monitoring and management of environmental pollutions, Nova Science Publishers, Inc. Hauppauge New York 1–638
15. El Nemr A (2012) Environmental pollutions and its relations to climate change. Nova Science Publishers, Inc. Hauppauge New York 1–694
16. Onyancha RB, Aigbe UO, Ukhurebor KE, Muchiri PW (2021) Facile synthesis and applications of carbon nanotubes in heavy-metal remediations and biomedical fields: a comprehensive review. *J Mol Struct* 1238:130462
17. Onyancha RB, Ukhurebor KE, Aigbe UO, Osibote OA, Kusuma HS, Darmokoesoemo H, Balogun VA (2021) A systematic review on the detections and monitoring of toxic gases using carbon nanotube-based biosensors. *Sens Bio-Sens Res* 34:100463
18. Ukhurebor KE, Athar H, Adetunji CO, Aigbe UO, Onyancha RB, Abifarini O (2021) Environmental implications of petroleum spillages in the Niger Delta regions of Nigeria: a review. *J Environ Manag* 293:112872
19. Ukhurebor KE, Aidonjio PA (2021) The influence of climate change on food innovations technology: review on topical developments and legal framework. *Agric Food Secur* 10(50):1–14
20. Kerry RG, Ukhurebor KE, Kumari S, Maurya GK, Patra S, Panigrahi B, Majhi S, Rout JR, Rodriguez-Torres MDP, Das G, Shin H-S, Patra JK (2021) A comprehensive review on the applications of nano-biosensor based approaches for non-communicable and communicable disease detection. *Biomater Sci* 9:3576–3602
21. Ukhurebor KE, Singh KRB, Nayak V, UK-Eghonghon G, (2021) Influence of SARS-CoV-2 pandemic: a review from the climate change perspective. *Environ Sci Process Impacts* 23:1060–1078
22. Gupta H, Parag R, Gogate PR (2016) Intensified removal of copper from waste water using activated watermelon based biosorbent in the presence of ultrasound. *Ultrason Sonochem* 30:113–122
23. Khan FSA, Mubarak N, Tan YH, Karri RR, Khalid M, Walvekar R, Abdullah EC, Mazari SA, Nizamuddin S (2020) Magnetic nanoparticles incorporation into different substrates for dyes and heavy metals removal—a review. *Environ Sci Pollut Res* 27:43526–43541. <https://doi.org/10.1007/s11356-020-10482-z>

24. Khan FSA, Mubarak NM, Khalid M, Walvekar R, Abdullah EC, Mazari SA, Nizamuddin S, Karri RR (2020) Magnetic nanoadsorbents' potential route for heavy metals removal—a review. *Environ Sci Pollut Res* 27:24342–24356. <https://doi.org/10.1007/s11356-020-08711-6>
25. Khan FSA, Mubarak NM, Tan YH, Khalid M, Karri RR, Walvekar R, Abdullah EC, Nizamuddin S, Mazari SA (2021) A comprehensive review on magnetic carbon nanotubes and carbon nanotube-based buckypaper for removal of heavy metals and dyes. *J Hazard Mater* 413:125375. <https://doi.org/10.1016/j.jhazmat.2021.125375>
26. Salem DMSA, Khaled A, El Nemr A, El-Sikaily A (2014) Comprehensive risk assessment of heavy metals in surface sediments along the Egyptian Red Sea coast. *Egypt J Aquat Res* 40:349–362. <https://doi.org/10.1016/j.ejar.2014.11.004>
27. Doebrich J, Linda Masonic L (2009) Copper - a metal for the ages. United States Geological Survey, Fact Sheet 2009–3031, May 2009. <https://pubs.usgs.gov/fs/2009/3031/FS2009-3031>
28. Phuengphai P, Singjanusong T, Kheangkhum N, Amnuay Wattanakornsiri A (2021) Removal of copper(II) from aqueous solutions using chemically modified fruit peels as efficient low-cost biosorbents. *Water Sci Eng* 14(4):286–294. <https://doi.org/10.1016/j.wse.2021.08.003>
29. El-Nemr MA, Aigbe UO, Hassaan MA, Ukhurebor KE, Ragab S, Onyancha RB, Osibote OA, El Nemr A (2022) The use of biochar-NH₂ produced from watermelon peels as a natural adsorbent for the removal of Cu(II) ions from water. *Biomass Convers Biorefin*. <https://doi.org/10.1007/s13399-022-02327-1>
30. Eldeeb TM, El-Nemr A, Khedr MH, El-Dek SI (2021) Novel bio-nanocomposite for efficient copper removal. *Egypt J Aquat Res* 47(3):261–267. <https://doi.org/10.1016/J.EJAR.2021.07.002>
31. El-Sikaily A, El Nemr A, Khaled A (2011) Copper sorptions onto dried red alga *Pterocladia capillacea* and its activated carbon. *Chem Eng J* 168:707–714. <https://doi.org/10.1016/J.ARABJC.2011.01.016>
32. Villen-Guzman M, Gutierrez-Pinilla D, Gomez-Lahoz C, Vereda-Alonso C, Rodriguez-Maroto JM, Arhoun B (2019) Optimizations of Ni(II) biosorptions from aqueous solutions on modified lemon peel. *Environ Res* 179:108849. <https://doi.org/10.1016/j.envres.2019.108849>
33. Ngabura M, Hussain SA, Ghani WAWA, Jami MS, Tan YP (2018) Utilizations of renewable durian peels for biosorptions of zinc from wastewater. *J Environ Chem Eng* 6(2):2528–2539. <https://doi.org/10.1016/j.jece.2018.03.052>
34. Alghamdi MM, El-Zahhar AA, Idris AM, Sadi TO, Sahlabji T, El Nemr A (2019) Synthesis, characterizations and applications of a new polymeric-clay-magnetite composite resin for water softening. *Sep Purif Technol* 224:356–365. <https://doi.org/10.1016/j.seppur.2019.05.037>
35. Chen Q, Yao Y, Li X, Lu J, Zhou J, Huang Z (2018) Comparison of heavy metal removals from aqueous solutions by chemical precipitations and characteristics of precipitates. *J Water Process Eng* 26:289–300. <https://doi.org/10.1016/j.jwpe.2018.11.003>
36. Wu H, Wang W, Huang Y, Han G, Yang S, Su S, Sana H, Peng W, Cao Y, Liu J (2019) Comprehensive evaluations on a prospective precipitations-flotations process for metal-ions removal from wastewater simulants. *J Hazard Mater* 371:592–602. <https://doi.org/10.1016/j.jhazmat.2019.03.048>
37. Yesil H, Tugtas AE (2019) Removal of heavy metals from leaching effluents of sewage sludge via supported liquid membranes. *Sci Total Environ* 693:133608. <https://doi.org/10.1016/j.scitotenv.2019.133608>
38. Guyo U, Mhonyera J, Moyo M (2015) Pb(II) adsorptions from aqueous solutions by raw and treated biomass of maize stover: a comparative study. *Process Safety Environ Protect* 93:192–200. <https://doi.org/10.1016/J.PSEP.2014.06.009>
39. Keawkim K, Khamthip A (2018) Removal of Pb²⁺ ions from industrial wastewater by new efficient biosorbents of oyster plant (*Tridacna patula*) and Negkassar leaf (*Mammea siamensis* T. Anderson). *Chiang Mai J Sci* 45(1):369–379
40. Sun H, Xia N, Liu Z, Kong F, Wang S (2019) Removal of copper and cadmium ions from alkaline solutions using chitosan-tannin functional paper materials as adsorbent. *Chemosphere* 236:124370
41. Manzoor Q, Nadeem R, Iqbal M, Saeed R, Ansari TM (2013) Organic acids pretreatment effect on Rosa bourbonia phyto-biomass for removal of Pb(II) and Cu(II) from aqueous media. *Bioresour Technol* 132:446–452
42. Ben-Ali S, Jaouali I, Souissi-Najar S, Ouederni A (2017) Characterizations and adsorptions capacity of raw pomegranate peel biosorbent for copper removal. *J Cleaner Product* 142:3809–3821
43. Tasao P (2014) Adsorptions of copper using pomelo peel and depectinated pomelo peel. *J Clean Energy Tech* 2(2):154–157
44. Romero-Cano LA, García-Rosero H, Gonzalez-Gutierrez LV, Baldeño-Pérez LA, Carrasco-Marín F (2017) Functionalized adsorbents prepared from fruit peels: equilibrium, kinetic and thermodynamic studies for copper adsorptions in aqueous solutions. *J Cleaner Prod* 162:195–204
45. Safari E, Rahemi N, Kahforoushan D, Allahyari S (2019) Copper adsorptive removal from aqueous solutions by orange peel residue carbon nanoparticles synthesized by combustions method using response surface methodology. *J Environ Chem Eng* 7(1):102847
46. Semerciöz AS, Göğüş F, Çelekli A, Bozkurt H (2017) Development of carbonaceous material from grapefruit peel with microwave implemented-low temperature hydrothermal carbonization technique for the adsorptions of Cu (II). *J Cleaner Prod* 165:599–610
47. Zhang W, Song J, He Q, Wang H, Lyu W, Feng H, Xiong W, Guo W, Wu J, Chen L (2020) Novel pectin based composite hydrogel derived from grapefruit peel for enhanced Cu(II) removal. *J Hazard Mater* 384:121445
48. El-Nemr MA, Abdelmonem NM, Ismail IM, Ragab S, El Nemr A (2020) Ozone and ammonium hydroxide modifications of biochar prepared from *Pisum sativum* peels improves the adsorption of copper (II) from an aqueous medium. *Environ Process* 7(3):973–1007. <https://doi.org/10.1007/s40710-020-00455-2>
49. Lingamdinne LP, Choi J-S, Angaru GKR, Karri RR, Yang J-K, Chang Y-Y, Koduru JR (2022) Magnetic-watermelon rinds biochar for uranium-contaminated water treatment using an electromagnetic semi-batch column with removal mechanistic investigations. *Chemosphere* 286(2):131776. <https://doi.org/10.1016/j.chemosphere.2021.131776>
50. Hairuddin MN, Mubarak NM, Khali M, Abdullah EC, Walvekar R, Karri RR (2019) Magnetic palm kernel biochar potential route for phenol removal from wastewater. *Environ Sci Pollut Res* 26:35183–35197. <https://doi.org/10.1007/s11356-019-06524-w>
51. Gregg SJ, Sing KSW (1982) Adsorptions surface area and porosity, 2nd edn. Academic Press INC, London
52. Rouquerol F, Rouquerol J, Sing KSW (1999) Adsorptions by powders and porous solids. Academic Press INC, London
53. Barrett EP, Joyner LG, Halenda PP (1951) The determination of pore volume and area distributions in porous substances. I. Computations from nitrogen isotherms. *J Amer Chem Soc* 73:373–380
54. Serag E, El Nemr A, El-Maghraby A (2017) Synthesis of highly effective novel graphene oxide-polyethylene glycol-polyvinyl alcohol nanocomposite hydrogel for copper removal. *J Water Environ Nanotech* 2(4):223–234
55. Botha N, Inglis HM, Coetzer R, Labuschagne FJW (2021) Statistical design of experiments: an introductory case study for polymer composites manufacturing applications. *MATEC Web of Conf* 347:00028. <http://hdl.handle.net/10204/12191>. Accessed 17 June 2022
56. Salem AMS, Harraz FA, El-Sheikh SM, Hafez HS, Ibrahim IA, Abdel Mottaleb MSA (2015) Enhanced electrical and luminescent performance of porous silicon/MEH-PPV, nanohybrid synthesized

- by anodizations and repeated spin coating. RSC Adv 5:99892–99898. <https://doi.org/10.1039/C5RA18407J>
57. Pattnaik D, Kumar S, Bhuyan SK, Mishra SC (2018) Effect of carbonizations temperatures on biochar formations of bamboo leaves. Mater Sci Eng 338:012054
 58. El-Nemr MA, Abdelmonem NM, Ismail IMA, Ragab S, El Nemr A (2020) The efficient removal of the hazardous Azo Dye Acid Orange 7 from water using modified biochar from Pea peels. Desal Water Treat 203:327–355
 59. El-Nemr MA, Abdelmonem NM, Ismail IMA, Ragab S, El Nemr A (2020) Removal of acid yellow 11 dye using novel modified biochar derived from watermelon peels. Desal Water Treat 203:403–431
 60. El-Nemr MA, Ismail IMA, Abdelmonem NM, El Nemr A, Ragab S (2021) Aminations of biochar derived from watermelon peel by triethylenetetramine and ammonium hydroxide for toxic chromium removal enhancement. Chinese J Chem Eng 36:199–222. S1004–9541(20)30464-X
 61. Slaný M, Jankovič L, Madejová J (2019) Structural characterization of organo-montmorillonites prepared from a series of primary alkylamines salts: mid-IR and near-IR study. Appl Clay Sci 176:11–20
 62. Hassaan MA, El Nemr A, Elkatory MR, Ragab S, El-Nemr MA, Pantaleo A (2021) Synthesis, characterization, and synergistic effects of modified biochar in combination with α -Fe₂O₃ NPs on biogas production from red algae *Pterocladia capillacea*. Sustainability 13(16):9275
 63. Bansal M, Mudhoo A, Garg VK, Singh D (2014) Preparations and characterizations of biosorbents and copper sequestrations from simulated wastewater. Int J Environ Sci Technol 11:1399–1412
 64. Larous S, Meniai AH (2012) Removal of copper (II) from aqueous solutions by agricultural by-products-sawdust. Energy Procedia 18:915–923
 65. Kovacova Z, Demcak S, Balintova M, Pla C, Zinicovscaia I (2020) Influence of wooden sawdust treatments on Cu(II) and Zn(II) removal from water. Mater 13:3575
 66. Luo H, Liu Y, Lu H, Fang Q, Rong H (2021) Efficient adsorption of tetracycline from aqueous solutions by modified alginate beads after the removal of Cu(II) ions. ACS Omega 6(9):6240–6251
 67. Eldeeb TM, Aigbe UO, Ukhurebor KE, Onyancha RB, El-Nemr MA, Hassaan MA, Osibote OA, Ragab S, Okundaye B, Balogun VA, El Nemr A (2022) Biosorption of Acid Brown 14 dye to mandarin-CO-TETA derived from mandarin peels. Biomass Convers Biorefin 1–21. <https://doi.org/10.1007/s13399-022-02664-1>
 68. Fotsing PN, Woumfo ED, Măicăneanu SA, Vieillard J, Tcheka C, Ngueagni PT, Siéwé JM (2020) Removal of Cu (II) from aqueous solutions using a composite made from cocoa cortex and sodium alginate. Environ Sci Poll Res 27:8451–8466. <https://doi.org/10.1007/s11356-019-07206-3>
 69. Ezeonuegbu BA, Machido DA, Whong CM, Japhet WS, Alexiou A, Elazab ST, Qusty N, Yaro CA, Batiha GES (2021) Agricultural waste of sugarcane bagasse as efficient adsorbent for lead and nickel removal from untreated wastewater: biosorptions, equilibrium isotherms, kinetics and desorptions studies. Biotechnol Rep 30:e00614
 70. Edet UA, Ifelebuegu AO (2020) Kinetics, isotherms, and thermodynamic modeling of the adsorption of phosphates from model wastewater using recycled brick waste. Processes 8(6):665
 71. Yu B, Zhang Y, Shukla A, Shukla SS, Dorris KL (2000) The removal of heavy metal from aqueous solutions by sawdust adsorptions—removal of copper. J Hazard Mater 80:33–42
 72. Răpă M, Țurcanu AA, Matei E, Predescu AM, Pantilimon MC, Coman G, Predescu C (2021) Adsorptions of copper (II) from aqueous solutions with alginate/clay hybrid materials. Mater 14:7187
 73. Pesic B (2017) Removal of heavy metals from water by wood-based lignocellulocis materials. WIT Trans Ecol Environ 220:81–91
 74. Sciban M, Klasnja M (2004) Study of the adsorptions of copper(II) ions from water onto wood sawdust, pulp and lignin. Adsorpt Sci Technol 22:195–206
 75. Leiva E, Tapia C, Rodríguez C (2021) Highly efficient removal of Cu(II) ions from acidic aqueous solutions using ZnO nanoparticles as nano-adsorbents. Water 13:2960
 76. Amrhar O, Nassali H, Elyoubi MS (2015) Application of nonlinear regression analysis to select the optimum absorption isotherm for methylene blue adsorption onto natural illitic clay. Bull Soc Roy Sci Liège 84:116–130
 77. Majd MM, Kordzadeh-Kermani V, Ghalandari V, Askari A, Silanpää M (2021) Adsorption isotherm models: a comprehensive and systematic review (2010– 2020). Sci Total Environ 151334. <https://doi.org/10.1016/j.scitotenv.2021.151334>
 78. Dehghani MH, Salari M, Karri RR, Hamidi F, Bahadori R (2021) Process modeling of municipal solid waste compost ash for reactive red 198 dye adsorption from wastewater using data driven approaches. Sci Rep 11(1):1–20. <https://doi.org/10.1038/s41598-021-90914-z>
 79. Zhang G, Liu N, Luo Y, Zhang H, Su L, Oh K, Cheng H (2021) Efficient removal of Cu (II), Zn (II), and Cd (II) from aqueous solutions by a mineral-rich biochar derived from a spent mushroom (*Agaricus bisporus*) substrate. Materials 14:35
 80. Bai X, Xing L, Liu N, Ma N, Huang K, Wu D, Yin M, Jiang K (2021) Humulus scandens-derived biochars for the effective removal of heavy metal ions: isotherm/kinetic study, column adsorptions and mechanism investigations. Nanomaterials 11:3255
 81. Khan TA, Mukhlif AA, Khan EA (2017) Uptake of Cu²⁺ and Zn²⁺ from simulated wastewater using muskmelon peel biochar: isotherm and kinetic studies. Egypt J Basic Appl Sci 4:236–248
 82. Hu X, Song J, Wang H, Zhang W, Wang B, Lyu W, Wang Q, Liu P, Chen L, Xing J (2019) Adsorptions of Cr(VI) and Cu(II) from aqueous solutions by biochar derived from *Chaenomeles sinensis* seed. Water Sci Tech 80:2260–2272
 83. Nagy B, Mânzatu C, Măicăneanu A, Indolean C, Barbu-Tudoran L, Majdik C (2017) Linear and nonlinear regression analysis for heavy metals removal using *Agaricus bisporus* macrofungus. Arab J Chem 10:S3569–S3579
 84. Jasper EE, Ajibola VO, Onwuka JC (2020) Nonlinear regression analysis of the sorption of crystal violet and methylene blue from aqueous solutions onto an agro-waste derived activated carbon. Appl Water Sci 10(6):1–11
 85. Tejada-Tovar C, Villabona-Ortiz A, Ortega-Toro R, Mancilla-Bonilla H, Espinoza-León F (2021) Potential use of residual sawdust of eucalyptus globulus labill in Pb (II) adsorptions: modelling of the kinetics and equilibrium. Appl Sci 11:3125
 86. Sachan D, Das G (2022) Fabrications of biochar-impregnated MnO₂ nanocomposite: characterizations and potential applications in copper (II) and zinc (II) adsorptions. J Hazard Toxic Rad Waste 26:04021049
 87. Rahim ARA, Johari K, Shehzad N, Saman N, Mat H (2020) Conversions of coconut waste into cost effective adsorbent for Cu(II) and Ni(II) removal from aqueous solutions. Environ Eng Res 26:200250
 88. Amirov N, Vakhshouri AR (2020) Numerical modelling and optimizations of product selectivity and catalyst activity in Fischer-Tropsch synthesis via response surface methodology: cobalt carbide particle size and H₂/CO ratio effects. Inter J Hydrogen Energy 45:31913–31925
 89. Isam M, Baloo L, Kutty SRM, Yavari S (2019) Optimisations and modelling of Pb(II) and Cu(II) biosorptions onto red algae

- (*Gracilaria changii*) by using response surface methodology. *Water* 11:2325
90. Sawood GM, Mishra A, Gupta SK (2021) Optimizations of arsenate adsorptions over aluminum-impregnated tea waste biochar using RSM–central composite design and adsorptions mechanism. *J Hazard Toxic Rad Waste* 25:04020075
 91. Dil EA, Ghaedi M, Asfaram A (2019) Applications of hydrophobic deep eutectic solvent as the carrier for ferrofluid: a novel strategy for pre-concentrations and determinations of mefenamic acid in human urine samples by high performance liquid chromatography under experimental design optimizations. *Talanta* 202:526–530. <https://doi.org/10.1016/j.talanta.2019.05.027>
 92. Bagheri R, Ghaedi M, Asfaram A, Dil EA, Javadian H (2019) RSM-CCD design of malachite green adsorptions onto activated carbon with multimodal pore size distributions prepared from *Amygdalus scoparia*: kinetic and isotherm studies. *Polyhedron* 171:464–472. <https://doi.org/10.1016/j.poly.2019.07.037>
 93. Mondal NK, Samanta A, Roy P, Das B (2019) Optimizations study of adsorptions parameters for removal of Cr(VI) using *Magnolia* leaf biomass by response surface methodology. *Sustain Water Resour Manag* 5:1627–1639. <https://doi.org/10.1007/s40899-019-00322-5>
 94. Roy P, Dey U, Chattoraj S, Mukhopadhyay D, Mondal NK (2017) Modeling of the adsorptive removal of arsenic(III) using plant biomass: a bioremedial approach. *Appl Water Sci* 7:1307–1321. <https://doi.org/10.1007/s13201-015-0339-2>
 95. Lingamdinne LP, Koduru JR, Chang YY, Karri RR (2018) Process optimizations and adsorptions modeling of Pb(II) on nickel ferrite-reduced graphene oxide nano-composite. *J Mol Liq* 250:202–211. <https://doi.org/10.1016/J.MOLLIQ.2017.11.174>
 96. Aigbe UO, Ukhurebor KE, Onyancha RB, Okundaye B, Pal K, Osibote OA, Esiekpe EL, Kusuma HS, Darmokoesoemo H (2022) A facile review on the sorptions of heavy metals and dyes using bionsanocomposites. *Adsorp Sci Tech* 8030175:1–36. <https://doi.org/10.1155/2022/8030175>

Publisher's note Springer Nature remains neutral with regard to jurisdictional claims in published maps and institutional affiliations.

Authors and Affiliations

Ahmed Eleryan¹ · Uyiosa O. Aigbe² · Kingsley E. Ukhurebor³ · Robert B. Onyancha⁴ · Tarek M. Eldeeb¹ · Mohamed A. El-Nemr⁵ · Mohamed A. Hassaan¹ · Safaa Ragab¹ · Otolorin A. Osibote² · Heri S. Kusuma⁶ · Handoko Darmokoesoemo⁷ · Ahmed El Nemr¹ 

Ahmed Eleryan
aeleryan71@yahoo.com

Uyiosa O. Aigbe
uyi4we@gmail.com

Kingsley E. Ukhurebor
ukeghonghon@gmail.com

Robert B. Onyancha
08muma@gmail.com

Tarek M. Eldeeb
tarikeldeeb77@yahoo.com

Mohamed A. El-Nemr
mohamedelnemr1992@yahoo.com

Mohamed A. Hassaan
mhss95@mail.com

Safaa Ragab
safaa_ragab65@yahoo.com

Otolorin A. Osibote
osibotea@cput.ac.za

Heri S. Kusuma
heriseptyakusuma@gmail.com

Handoko Darmokoesoemo
handoko.darmokoesoemo@gmail.com

- ¹ Environment Divisions, National Institute of Oceanography and Fisheries (NIOF), Kayet Bey, Elanfoushy, Alexandria, Egypt
- ² Department of Mathematics and Physics, Faculty of Applied Sciences, Cape Peninsula University of Technology, Cape Town, South Africa
- ³ Department of Physics, Faculty of Science, Edo State University Uzairue, Okpella, Edo State, Nigeria
- ⁴ Department of Technical and Applied Physics, School of Physics and Earth Sciences Technology, Technical University of Kenya, Nairobi, Kenya
- ⁵ Department of Chemical Engineering, Faculty of Engineering, Minia University, Minia, Egypt
- ⁶ Department of Chemical Engineering, Faculty of Industrial Technology, Universitas Pembangunan Nasional Veteran Yogyakarta, Sleman, Indonesia
- ⁷ Department of Chemistry, Faculty of Science and Technology, Airlangga University, Mulyorejo, Surabaya 60115, Indonesia